https://doi.org/10.5194/egusphere-2026-4031
Preprint. Discussion started: 15 July 2026

Drivers of net community production in the bottom of Arctic pack ice

*Rosalie McKay[1], Zoe Koenig[1], Polona Itkin[2], Rolf Gradinger[1], Christien Laber[1], Janina Osanen[3], Sanna Saur Heiland[1], Karley Campbell[1]

[1]Department of Arctic and Marine Biology, UiT The Arctic University of Norway, Tromsø, Norway
[2]Norwegian Polar Institute, Tromsø, Norway
[3]Department of Biology, Norwegian University of Science and Technology, Trondheim, Norway

*corresponding author: rosalie.d.mckay@uit.no

Short Plain Language Summary <500-character (incl. spaces)

We investigate how sea-ice algal communities and photosynthesis are influenced by nutrients deeper in the water column north of Svalbard. A storm increased ocean mixing, bringing more nutrients and heat to the ice, which had competing effects of supporting photosynthesis and of accelerating ice melt. The storm also reduced light for algal growth by depositing more snow on the ice. Short-term physical forcing can strongly influence sea-ice algal production through multiple interacting processes.

Abstract

The availability of nutrients to sea-ice microbial communities varies as drifting pack ice traverses distinct hydrographic regimes and experiences episodic mixing events. Vertical turbulent fluxes generated by processes such as ice movement and wind can enhance nutrient resupply at the ice–ocean interface, potentially influencing community composition and net community production. In this study, we evaluate the relationships between bottom sea-ice algal communities and oceanic conditions during a sea-ice drift study north of Svalbard, which crossed different branches of the Atlantic Water inflow to the Arctic over the Yermak Plateau and the Sofia Deep. Despite elevated nitrate concentrations in under-ice waters associated with the Svalbard Branch of Atlantic Water inflow, the largest nutrient and heat fluxes to the bottom ice occurred during a storm event. These fluxes coincided with increased biomass-specific net community productivity but also enhanced algal biomass loss through melt. At the same time, snow redistribution during the storm increased snow depths and reduced light availability at the bottom ice, affecting net community production. Independent of nutrient conditions, the transition from net heterotrophy (oxygen consumption) to net autotrophy (oxygen production) occurred when under-ice transmitted photosynthetically active radiation exceeded a daily range of 1.1 to 3.5 µmol m^{-2} s^{-1}. Although nutrient supply remains important, our results suggest that light availability may exert a stronger control on sea-ice net community production than nutrient supply when nutrients are not critically depleted. We further highlight the importance of episodic storm events in modifying nutrient and heat vertical fluxes, and light availability at the ice–ocean interface, thereby contributing to regional variability in ice algal bloom dynamics.

https://doi.org/10.5194/egusphere-2026-4031
Preprint. Discussion started: 15 July 2026

1. Introduction

Pack ice is a highly dynamic environment, where variable light and nutrient supply directly control sea-ice algal production and the carbon biomass that fuels ice-associated food webs (Gradinger and Bluhm, 2020; Koch, 2023). The balance between primary production and respiration by ice-associated biota, including bacteria, algae and metazoa, defines sea ice net community production (NCP). Strong stratification at the halocline in the Arctic can prevent nutrients from reaching the algae which tend to concentrate in the bottom ice, limiting or terminating their growth (Aagaard et al., 1981; Anderson et al., 2013; Smith et al., 2025). Sea-ice communities in this region persist under low-light and nutrient-limited conditions, with primary production rates in the Eurasian Basin typically ranging from 0.1 to 13 mg C m^{-2} d^{-1} (Assmy et al., 2013; Fernández-Méndez et al., 2014; Fernández-Méndez et al., 2015). As the ice drifts from the central basin toward the Yermak Plateau, enhanced nutrient supply may support higher productivity, with the limited available observations reporting rates of 3.7–34.5 mg C m^{-2} d^{-1} (Ehrlich et al., 2021).

Conditions at the ice–ocean interface are highly variable as seasons change and pack ice drifts across different water masses (Fong et al., 2024). The mobility of Arctic pack ice is governed by large-scale advection and small-scale mechanical redistribution, including divergence and convergence, resulting in a highly dynamic ice cover (Lei et al., 2022; Salganik et al., 2023; von Albedyll et al., 2024). This variability spans a hierarchy of spatial scales, from regional atmospheric and oceanographic processes (10–100 km), to floe-scale heterogeneity associated with leads, ridges, and individual ice floes (100 m–1 km) (McNutt & Overland, 2003), and local variations in snow cover driven by atmospheric turbulence and sea-ice roughness (1–10 m) (Itkin et al., 2023). Together, these interacting processes create a highly heterogeneous habitat for ice-associated algae, generating substantial spatial variability in biomass and productivity and complicating the collection of representative bottom-ice samples (Lange et al., 2017). Such variability is particularly pronounced north of Svalbard, where drifting sea ice encounters contrasting oceanographic regimes.

Sea ice dynamics in the region North of Svalbard are heavily influenced by the advection of Atlantic Water (AW). The AW flows northwards along the western slope of Svalbard and then veers eastward once reaching the northwestern tip of Svalbard (Kolås et al., 2020). These shallow, warm, salty, and nutrient rich waters occupy the subsurface beneath colder and fresher Polar Surface Water, which is overlain by sea ice transported from the central Arctic Ocean via the Transpolar Drift. Originating on the Siberian shelves, this drift carries sea ice and surface waters across the Arctic Basin toward Fram Strait. Consequently, the supply of nutrients to sea-ice communities depends on processes that transfer nutrients from the underlying AW across the stratified upper water column into the surface mixed layer and toward the ice–ocean interface.

There are several mechanisms that impact mixing dynamics beneath sea ice, which have the potential to impact bottom-ice algal communities. Localized mixing driven by topography and atmospheric forcing are thought to increase nutrient availability in surface waters adjacent to and beneath sea ice. These mixing hotspots have been suggested as a source of nutrient replenished surface waters (Dalman et al., 2019; Duarte et al., 2021; Castellani et al., 2026). Additionally, storms are a major source of energy for the ocean, generating large levels of turbulence and mixing in the upper ocean (Cohen 2017), changes in the ice boundary layer conditions and increased deeper water mixing towards the ice (Castro de la Guardia et al., 2019). Vertical turbulent fluxes generated by processes such as ice movement and wind can also enhance nutrient resupply at the ice–ocean interface (Peterson et al., 2017).

https://doi.org/10.5194/egusphere-2026-4031
Preprint. Discussion started: 15 July 2026

In the context of climate change, the ongoing Atlantification of the eastern Eurasian Basin, driven by an increasing inflow of AW (Polyakov et al., 2017), is transforming Arctic marine ecosystems. The region north of Svalbard, where sea ice–ocean processes are already strongly influenced by AW, therefore serves as an important early indicator of ecosystem and oceanographic changes that may eventually spread further into the Arctic Ocean. This progression is likely to be accompanied by increased open water and storm activity under continued warming (Graham et al., 2019; Crawford et al., 2022), potentially leading to more frequent and intense mixing. Arctic cyclones are increasing in frequency and may be important contributors to the observed loss of Arctic sea ice (Cavallo et al., 2025). Concurrently, a shift toward increasing first-year ice (FYI) relative to second-year ice (SYI) alters ice bulk salinity and snow cover, with evidence of effects on sea-ice algal communities (Campbell et al., 2022). As snow accumulation on sea ice strongly reduces light transmission to the bottom-ice habitat (Nicolaus et al., 2012; Perovich, 1996), these changes are expected to influence sea-ice algal primary production, which is often light-limited (Heorton et al., 2025; Leu et al., 2015). Indeed, much of the Arctic Ocean has become brighter owing to reduced snow and ice thickness, and the resulting increase in light transmission (Webster et al., 2026). However, the Atlantic sector remains an exception, where future changes in snow cover are more uncertain because increasing precipitation may lead to either greater snow accumulation or more frequent rainfall events (Merkouriadi et al., 2017).

To better understand how under-ice turbulence and atmospheric forcing alter the balance between autotrophic and heterotrophic processes at the floe scale, we conducted a 10–day ice drift study in May 2023. The study captured a storm event during spring sea-ice algal growth in a region influenced by AW, allowing us to assess the biological consequences of storm-driven changes in snow cover, light availability, and exchange across the ice–ocean interface. Through linking field data with laboratory studies, we extended NCP determination across our sampling area on the floe.

2. Materials and Methods

2.1. Field sites

The study was conducted within a region of consolidated sea ice surrounding the moored vessel over the eastern part of the Yermak Plateau north of Svalbard. The drift began at 80.999935° N, 9.475807° E on 17 May 2023, and was completed at 80.647532° N, 9.9684° E on 27 May 2023 (Fig. 1b). Sampling was conducted at three sites along the drift track: Site 1 (17–19 May) over the Yermak Plateau (950 m water depth), Site 2 (21 May) over the Sofia Deep (2000 m), and Site 3 (26–27 May) over the Svalbard continental slope (950 m) (Fig. 1). Based on the regional circulation of AW originating from the West Spitsbergen Current, different current branches were likely encountered during the study period (Koenig et al., 2017; Crews et al., 2019). Site 1, located west of the Sofia Deep over the Yermak Plateau, was most likely influenced by a combination of the Yermak Pass Branch and the Yermak Branch (Fig. 1a). Site 2 was likely influenced by recirculated AW within the Sofia Deep (Kolås et al., 2020). Site 3, located south of the Sofia Deep over the continental slope, was most likely influenced by the Svalbard Branch (Fig. 1a).

The study region of the floe had a size of ca 0.36 km^2 and consisted of both FYI and SYI. Sea-ice back-trajectory analyses (Fig. S1) and regional sea-ice transport patterns suggest that the oldest ice floes within the region likely originated from the Laptev Sea. We therefore infer that the SYI areas of the floe investigated here

https://doi.org/10.5194/egusphere-2026-4031
Preprint. Discussion started: 15 July 2026

was also likely formed in the Laptev Sea and at least some parts had survived at least one melt season. Standardized sea ice observations were taken in transit through the ice, both before and after sampling and logged into the Arctic Shipborne Sea Ice Standardization Tool (ASSIST; Norwegian Meteorological Institute). In the first phase of the sampling period the study floe drifted generally eastwards, alternating between southeast and northeast directions; a change to a southwest drift occurred on 25 May (Fig. 1b) in response to strong northerly winds (see below).

https://doi.org/10.5194/egusphere-2026-4031
Preprint. Discussion started: 15 July 2026

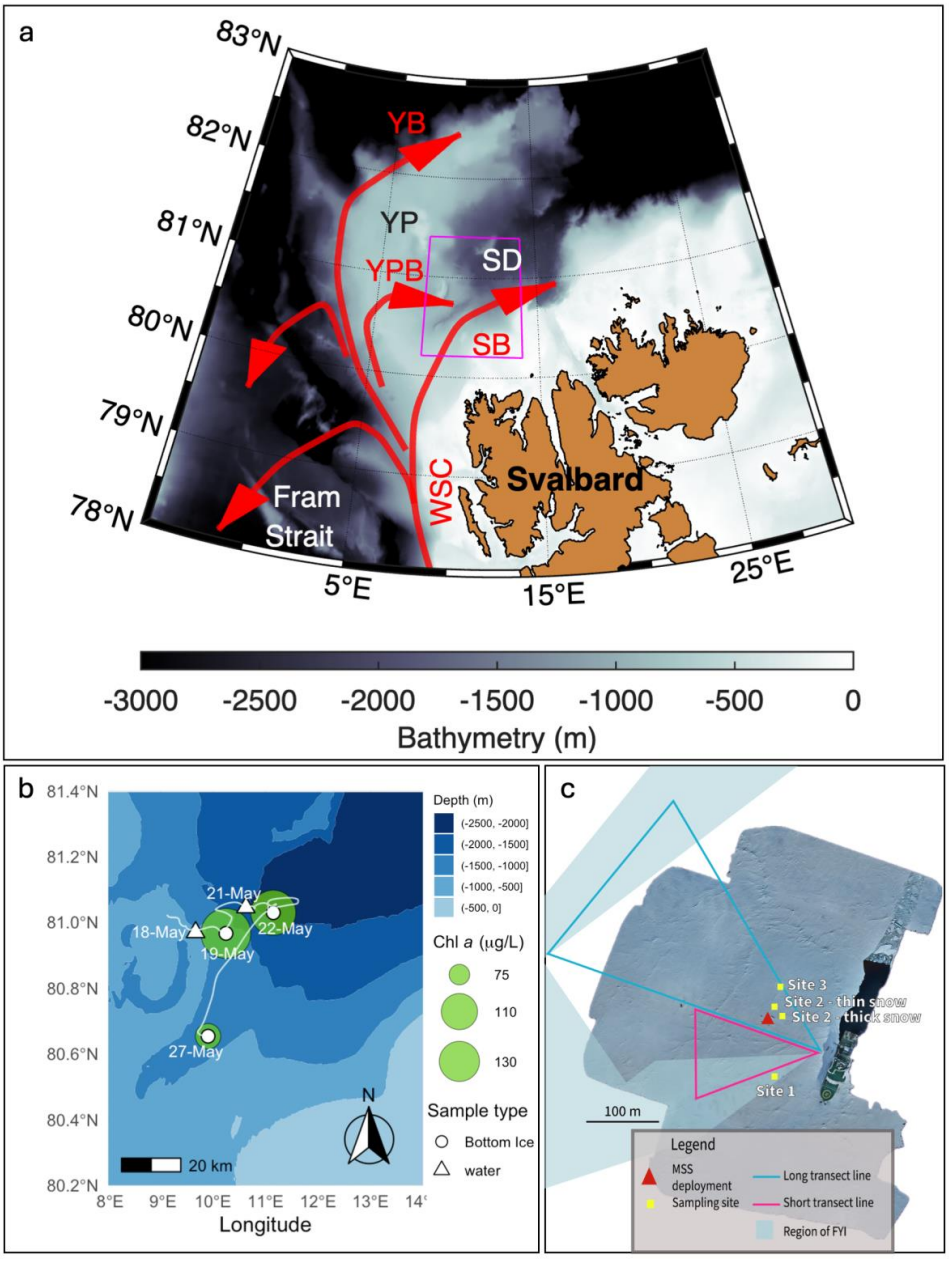

Figure 1: Study region and sites: (a) Circulation pattern of Atlantic Water around Svalbard, with the West Spitsbergen Current (WSC), the Svalbard Branch (SB), the Yermak Branch (YB) and the Yermak Pass Branch (YPB). Regions are denoted by Yermak Plateau (YP) and Sofia Deep (SD). Bathymetry is from the International Bathymetric Chart of the Arctic Ocean, IBCAO-v3 (Jakobsson et al., 2012). The pink box indicates the zoom in in panel (b) Figure adapted from Koenig et al. (2021). (b) Sampling locations, ice floe drift and chlorophyll *a* (chl *a*) in the bottom 5 cm of ice. The chl *a* concentration for 22 May is an average of the two sites sampled. Both

https://doi.org/10.5194/egusphere-2026-4031
Preprint. Discussion started: 15 July 2026

water and bottom ice were sampled 27 May. (c) Map of the sea ice sampling site distributions on the ice floe with locations of the MSS deployment and transect lines overlain on a drone photo taken 24 May. White areas were not covered in the drone image. Light blue shaded region shows first year ice (FYI), with remaining ice estimated as second year ice (SYI).

2.2. Sampling routine

Sampling of the sea ice and underlying water column down to 25 m depth was completed in approximately 100–120 m distance from RV *Kronprins Haakon* at three (Site 1, 2 and 3) different sites on the study floe (Fig. 1c). For each sample site, water collection was carried out on the first day, and ice and snow sampling on the second day, with day 3 dedicated to lab work. At Site 3, water and ice were sampled on the same day. Under-ice water was collected near-to the area of ice sampling but far enough away to prevent flooding of the ice-sampling site. Adverse weather conditions halted on-ice work between Sites 2 and 3, delaying the resumption of sampling. Due to drifting of the floe over time and the alternating days of sea ice and under-ice water collection, the coordinates of ice and water samples of each site differ (Table 1).

Table 1. Sampling dates and oceanographic settings for under-ice water collection and sea-ice sampling

Site	Date under–ice water collection	Date ice sampling	Localisation	Ocean Current
1	18 May	19 May	Yermak Plateau	Yermak Pass Branch and Yermak Branch
2 Thick snow	21 May	22 May	Sofia Deep	Atlantic Water Boundary current recirculation
2 Thin snow	21 May	22 May	Sofia Deep	Atlantic Water Boundary current recirculation
3	27 May	27 May	Svalbard continental slope	Svalbard Branch

2.3. Wind and hydrographic data

Atmospheric conditions were continuously recorded during the cruise by the ship's weather station. The wind speed and direction were recorded by a Vaisala WMT702 sensor on top of the mast (35 m). A Vaisala HMP155 meteorological temperature and humidity probe mounted on the bridge (13.5 m) recorded air temperatures.

Temperature, Salinity and Depth (CTD) profiles were obtained from 2 to 250 m depth using a Microstructure Sensor Profiler (MSS, Sea and Sun Technology) deployed from the ice (Koenig et al., 2023 and Schulz et al., 2024) at approximately 120 m away from the ship. MSS casts were completed daily from 18 May to 27 May, with no casts on 25 May, from the same ice hole maintained open under a tent (Fig. 1c). The profiler had precision conductivity, temperature, and pressure sensors as well as microstructure sensors including two airfoil shear probes, a fast response thermistor, and a micro conductivity sensor, all sampling at 1024 Hz. Data processing follows Meyer et al. (2017b). Final processed profiles include 0.1 m vertically averaged temperature and salinity, and 2–2.5 m vertical resolution turbulent dissipation rate estimates. Reported accuracies of the

https://doi.org/10.5194/egusphere-2026-4031
Preprint. Discussion started: 15 July 2026

sensors by the manufacturer were 0.1 m, 0.0028°C, and 0.003 mS cm^{-1} for depth, temperature, and conductivity, respectively. The estimated accuracy of the MSS salinity measurement is 0.01 on the practical salinity scale.

2.4. Ice and snow thickness, and floe-wide estimates

We characterized ice thickness and snow depth variations along two separate transects, 500 to 1100 m long, on the floe (Fig. 1c; short and long transects). Sea ice thickness was estimated by electromagnetic induction with a GEM–2 (Geophex Ltd) and snow thickness was measured by Magnaprobe (SnowHydro Ltd) (Itkin et al., 2023). For sea ice thickness, the footprint of the GEM–2 is several meters, with precision estimated to 0.1 m. The absolute precision may be affected by fast-fluctuating ambient temperatures that can influence the electromagnetic measurements. The GEM-2 data were calibrated using thickness measurements from drill holes at the coring sites (Itkin et al., 2025). Sea ice thickness was derived by subtracting the snow depth from the estimated snow and ice thickness, which was a direct point measurement. For the snow depth profiles, measurements were done every 1–1.5 m along the transect line (Fig. 1c).

Four snow pits were made to determine vertical profiles of snow temperature, structure and density (Macfarlane et al., 2023). The first was adjacent to the Site 1 ice sampling site, with three additional snow pits made near to the MSS deployment (Fig. 1c), two before the storm of different snow thicknesses and one after the storm. Sea-ice age was inferred from a combination of ice-core salinity profiles (Fig. S2) and snow-pit observations (Fig. S5). The lower salinities observed in the upper part of the ice cores are characteristic of SYI, reflecting desalination during at least one summer melt season. This interpretation is supported by the complex snow stratigraphy observed at the SYI site, which suggests snow accumulation predating the most recent freeze-up and the influence of multiple warm-air intrusion events during winter. This point information was then extrapolated to the entire sampling area based on the ice type areal coverage estimated from ship radar images (Fig. S3), drone orthophoto mosaics, snow depth and ice thickness collected along the transect lines (Fig. S6).

2.5. Determination of Photosynthetically Active Radiation (PAR) irradiance

Measurements of transmitted, surface downwelling and upwelling irradiance within the PAR spectral region (as photon flux density, µmol photons m^{-2} s^{-1}) were taken immediately prior to ice–core collection, corresponding to a local time between approximately 10:00 –14:00. Measurements were recorded with a LI–COR LI–1500 logger and the upwelling/downwelling surface irradiance was consecutively recorded using LI–COR LI–190R 2π quantum sensor approximately 0.6 m above the undisturbed snow surface and towards the sun. Under-ice transmitted irradiance was recorded using LI–193 4π underwater quantum sensor supported by a mechanical arm, which was positioned approximately 0.1 m below the ice–ocean interface and 1 m away from the deployment hole. Together the values from surface downwelling and under-ice transmitted irradiance were used to determine point measurements of transmittance (%).

The resultant transmittance values were subsequently used alongside hourly All Sky Surface Total PAR (MJ m^{-2} hr^{-1}) data (NASA Langley Research Center's Prediction Of Worldwide Energy Resources (POWER), version 2.5.22) to calculate hourly under-ice transmitted irradiance throughout the study period. Values were obtained from the period 19 May through 28 May, 2023 in local time using Latitude 80.9664 N and Longitude 10.2446 E, with the resolution of the model covering the full sampling area (Fig. S9). For each sampling site, modelled downwelling PAR was scaled using the ratio between in situ LICOR measurements and the corresponding

https://doi.org/10.5194/egusphere-2026-4031
Preprint. Discussion started: 15 July 2026

modelled downwelling value at the time of sampling. The resulting corrected hourly irradiance in the PAR range time series was combined with measured ice transmittance to estimate hourly under-ice transmitted irradiance.

2.6. Sample Collection

2.6.1. Water collection

During each water sampling event (May 18, 21, 24 and 27), discrete water samples were collected from zero (i.e. sea ice–ocean interface and hereafter referred to as interface water), 0.2, 1, 5, 10 and 25 m beneath the sea ice. The interface and 0.2 m water were collected using a peristaltic pump (Masterflex), while all other samples were obtained using a HYDRO–BIOS Ruttner water sampler.

Samples from all depths were analysed in triplicates for inorganic nutrient concentrations, including silicic acid ($Si(OH)_4$), nitrate and nitrite (NO_3+NO_2), and phosphate (PO_4). To assess whether nutrient concentrations in any interface water source were markedly different from the others, Dixon's Q tests were conducted separately for each nutrient (n=3) in R (version 2025.09.2+418) using the *outliers* package. The analysis was interpreted for differences in nutrient concentrations amongst potentially distinct water masses. Additional interface water was collected from each water sampling site and filtered through 0.2 µm (Millipore Express Plus Membrane) within 24 h of collection and stored in the dark at room temperature and hereafter referred to as FSW.

2.6.2. Sea ice coring

During each ice coring day (Site 1, 2 and 3) approximately twelve cores were collected using a 9 cm Mark II Kovacs core barrel. Sampling for biogeochemical analyses was focused to snow depths of 0.3 m or less, to ensure sufficient light for photosynthesis and make data from various sampling sites more comparable. These cores were collected and processed following a diluted melt procedure where the bottom 5 cm of ice of five to six ice cores were pooled together in insulated containers and melted in a dark Coleman cooler box over 24 h with FSW added at a volumetric ratio of three parts FSW to one part ice (Campbell et al., 2019). These salinity-buffered core sections are hereafter referred to as the bottom ice and are the basis of biogeochemical analyses within this study, including chl *a*, particulate organic carbon (POC), particulate organic nitrogen (PON), abundances by flow cytometry and light microscopy, and NCP. All reported data have been corrected for dilution by measuring the final melted volume and subtracting the volume of FSW added; the ratio of total to actual ice volume was then calculated accordingly.

Sea ice cores were also collected for assessment of bulk-ice nutrients and were melted without the addition of FSW. The bottom 0.1 m of these cores was sectioned at a 0.025 m resolution, then melted in darkness within vacuum sealed plastic bags (Menuett) at room temperature (Hu et al., 2018). Two cores were taken at approximately 9:00 local time during each sea ice sampling event to measure temperature and bulk salinity. Temperature was measured immediately after core retrieval using a Testo 720 with robust stainless-steel probe inserted a few centimeters into the ice, every 5 cm along the core. The salinity core was cut into sections of 0.1 m in length and were melted at room temperature before measurement (WTW Cond 3110 with a WTW TetraCon 325 probe).

https://doi.org/10.5194/egusphere-2026-4031
Preprint. Discussion started: 15 July 2026

2.7. Laboratory Procedures

2.7.1. Inorganic nutrients, chlorophyll *a*, and particulate organic carbon

Nutrient samples were filtered through combusted 0.7 µm Whatman GFF filters using a10% HCl washed syringe and Swinnex filter holder. The nutrient samples were stored at –20°C in 10% HCl acid washed polypropylene vials (Falcon) before analysis within four months on a Seal Analytical XY–2 Sampler QuAAtro 39 Continuous Segmented flow AutoAnalyzer and following thawing at 60°C for 15 mins (Cauwet, 1999; Hansen and Koroleff, 1999).

Chlorophyll *a*, POC and PON were subsampled by vacuum filtration onto non combusted (chl *a*) and combusted (POC/PON) 0.7 µm Whatman GFF filters, respectively. Chlorophyll *a* was determined in pseudo-duplicate by fluorescence following dark extraction in 90% acetone at 4°C for 18–24 hours. A Turner Designs Trilogy Fluorometer with Chl–A unit was used for measurement at room temperature of blank (90% acetone) corrected chl *a* fluorescence before and after acidification with 5% HCl (Strickland and Parsons, 1972). The POC/PON filters were frozen at –20°C before analysis within eighteen months. After thaw, they were dried for 24 hours in a 60°C oven before fuming in concentrated HCl for 24 hours to remove inorganic carbon, followed by an additional 24 hours in a 60°C oven. Filters were then packed into tin capsules and analysed on a Control Equipment Corporation 440 Elemental Analyzer (Gordon Jr., 1969).

2.7.2. Flow cytometry and microscopy

We defined algal size groups as microeukaryotes (20–200 µm), nanoeukaryotes (2 to 20 µm), and picoeukaryotes (less than 2 µm in size). The abundances of photosynthetic pico- and nanoeukaryotes were analysed by flow cytometry according to Gasol et al. (2016). Subsamples from interface water and diluted melt were fixed with glutaraldehyde to a final concentration of 0.1% and then stored at –80°C. Samples were analysed on a BD Accuri C6 Plus flow cytometer within seven months of collection. Algae populations were identified using forward scatter and red fluorescence.

Samples for determination of abundance and species composition of nano- and microeukaryotic algae in the diluted bottom-ice melt were fixed with acidic Lugol's solution at 0.4% concentration (Parsons et al., 1984) before storage at 4°C and analysed within one year of collection on a Leica Leitz DM IL inverted microscope. Ice algae were identified to the lowest possible taxonomic rank by size and morphology using Poulin and Cardinal (1983), Medlin and Priddle (1990), and Tomas (1997) as references. Due to preservation constraints, flagellated taxa were grouped into a single "flagellates" category for analysis. Cells were assigned to protist groups of pennate diatoms, centric diatoms, dinoflagellates, flagellates or other (Campbell et al., 2018).

2.7.3. Collection and growth of cultured algae

Additional NCP experiments were conducted on sea-ice algal species, that had been collected and isolated on the 2025 MicroSHIFT project cruise north of Svalbard and subsequently cultured at UiT The Arctic University of Norway. Mixed community cultures were collected from the bottom 0–5 cm of sea ice after slow thaw. Single cell algae isolates were extracted for monocultures of *Nitzschia frigida* and *Pseudonitzschia sp.* into sterile F/2 growth media containing silicic acid (Andersen, 2005). These were grown at 4°C (INCU–Line 150R Premium

https://doi.org/10.5194/egusphere-2026-4031
Preprint. Discussion started: 15 July 2026

Incubator) and 30 µmol photons m^{-2} s^{-1} for five months prior to use. These incubations were conducted to determine if highly abundant species within the most dominant functional group observed (pennate diatoms) in the ice would contribute differently to NCP rates.

2.7.4. Net community Production (NCP)

Following Campbell et al. (2016), oxygen-based photosynthesis-irradiance (PI) curves were constructed from incubations on the pooled bottom-ice samples and cultured algae. We modified the original procedure which used four 4500 ml incubation flasks to measure the rate of oxygen consumption or production (i.e. NCP) by using eight to ten 120 ml airtight glass bottles with Pyroscience robust oxygen optodes. Bottom-ice samples were incubated with light intensities ranging from 0 (dark bottle) to 240 µmol photons m^{-2} s^{-1} measured with a Walz US–SQS/L scalar PAR irradiance probe and logger (Walz model ULM–500). Bottom-ice samples were pre-filtered with 350 µm Nitex mesh to remove potential grazing organisms and incubations were 14–80 hours long.

For the cultured algae, experiments were conducted in exponential growth phase (Fig. S4), at a specific growth rate of 0.24 d^{-1}. Chlorophyll *a* concentration was determined at the time of transfer to the incubation bottles, with the exception that samples were not pre-filtered through Nitex mesh. Samples were incubated for 86 hours at seven light intensities ranging from 0 up to 327 µmol photons m^{-2} s^{-1}.

Oxygen optode sensors were calibrated prior to each incubation using 0% and 100% dissolved oxygen standards of 0.17 M sodium dithionite ($Na_2S_2O_4$) and air saturated seawater, respectively (Bagshaw et al., 2011). Temperature measurements within each incubation chamber were taken by a Pyro Science temperature probe and ranged from –1.1 to –1.4°C over the different sampling events but were constant throughout each incubation. The oxygen concentration was recorded for each bottle continuously at 2 second intervals under stirring, and hourly averages were calculated. The NCP for each bottle was calculated (µmol O_2 l^{-1} h^{-1}) from the slope of the linear change in oxygen concentrations from the starting concentration (T_0), with changes in the black bottle representing dark respiration.

2.8. Model fitting and estimates

2.8.1. Curve fitting for net community production

Photosynthesis–irradiance curves were fitted using non-linear least squares regression in Matlab version R2024b software, applying the exponential model of Jassby and Platt (1976), and the photoinhibition model of Platt et al. (1980) as modified by Arrigo et al. (2010). Photosynthetic parameters were calculated relative to chl *a* biomass for the bottom ice at each site and included:

P_S^*, maximum photosynthetic rate (mol O_2 [g chl *a*]$^{-1}$ h^{-1})

a^*, photosynthetic efficiency (mol O_2 [g chl *a*]$^{-1}$ h^{-1} [µmol photons m^{-2} s^{-1}]$^{-1}$)

P_0^*, uptake or release of O_2 at zero irradiance (mol O_2 [g chl *a*]$^{-1}$ h^{-1})

I_C, compensation irradiance (µmol photons m^{-2} s^{-1})

I_S, the photoacclimation parameter (µmol photons m^{-2} s^{-1})

β^*, photoinhibition effect (mol O_2 [g chl *a*]$^{-1}$ h^{-1} [µmol photons m^{-2} s^{-1}]$^{-1}$)

https://doi.org/10.5194/egusphere-2026-4031
Preprint. Discussion started: 15 July 2026

For the field data, hourly NCP rates were computed from transmitted PAR irradiance (Sect. 2.5) and the above exponential model (Arrigo et al., 2010) and summed over 24 h to obtain daily rates (mmol O_2 m^{-2} day^{-1}). Oxygen production values were converted to carbon fixation rates using a CO_2:O_2 ratio of 1.2, assuming 1.2 moles of CO_2 fixed per mole of O_2 produced (Fenchel and Glud, 2000). Carbon fixation rates were subsequently converted from molar units to milligrams of carbon.

2.8.2. Vertical flux estimation

The dissipation rate of turbulent kinetic energy per unit mass, ε, was estimated using the isotropic relation and by integrating the turbulent shear spectra. Shear spectra were calculated using record lengths of 6 s (sliding by 3 s) and FFT lengths of 2 s (50% overlapped). Vibration-coherent noise is removed using the method of Goodman et al. (2006). A final dissipation rate estimate is obtained by averaging the estimates from the two probes when they agree within 95% confidence intervals (Lueck et al., 2022), or the minimum estimate if they do not. The noise level of the dissipation rate measured by the MSS is about 1–3.10^{-9} W kg^{-1}. Ocean microstructure measurements are available from Koenig et al. (2026). The turbulent heat flux F_H (in W m^{-2}) was calculated as:

$$F_H = -\rho_0 C_p K_\rho \frac{\partial \theta}{\partial z} \quad (1)$$

Where ρ_0 = 1028kg m^{-3} is the seawater density, C_p = 3991.9J kg^{-1} K^{-1} is the specific heat of seawater, θ is the background temperature and K_ρ is the diapycnal eddy diffusivity. We thus assume that turbulence diffuses the fine scale temperature gradient at the same rate as the density gradient. The sign convention is that positive heat fluxes correspond to upward heat fluxes in the water column. An upper bound for diapycnal diffusivity was obtained using the Osborn (1980) relation:

$$K_\rho = \Gamma \frac{\epsilon}{N^2} \quad (2)$$

With the mixing coefficient set to Γ =0.2, the recommended value for the oceanic applications (Gregg et al., 2018). The buoyancy frequency or Brunt Vaisala frequency, N, was calculated using $N^2 = -\frac{g}{\rho_0}\frac{\partial \sigma_\theta}{\partial z}$ where g is the gravitational acceleration and σ_θ the potential density anomaly referenced to surface pressure. Background vertical gradients (for temperature and density) were taken over a 10 m length scale.

Using vertical gradients between successive depths of water sampling vertical separation, we obtain "coarse" turbulent fluxes of nitrate (here NO_3+NO_2). The coarse turbulent nitrate fluxes, F_{NO_3} (in µmol m^{-2} s^{-1}) are estimated as:

$$F_{NO_3} = -\rho_0 \underline{K_\rho} \frac{\Delta C_{NO_3}}{\Delta z} \quad (3)$$

Where C_{NO_3} is the nitrate concentration. To be consistent with the coarse vertical spacing between the consecutive sampling depths Δz of nitrate concentration estimates, $\underline{K_\rho}$ is obtained by averaging K_ρ over Δz. The discrete estimate of the gradient between two nitrate data points, $\frac{\Delta C_{NO_3}}{\Delta z}$, resulting estimates of nitrate fluxes are assigned to the mid-depth between two water sampling depths.

https://doi.org/10.5194/egusphere-2026-4031
Preprint. Discussion started: 15 July 2026

2.8.3. Floe wide net community production estimate

Provided the known link of NCP to light availability (Castellani et al., 2022), it is interesting to consider the metabolic balance of NCP at the floe scale. Following the exponential decay framework of Veyssière et al. (2022), total under-ice transmittance can be expressed as a function of snow, ice, and algal attenuation:

$$T_s = (1-\alpha_s)e^{-\kappa_s h_s - \kappa_i h_i - \kappa_B \delta_z} \quad (4)$$

Where κ_s is the snow extinction coefficient (m^{-1}), h_s the snow depth (m), T_s the light transmission, α_s the snow albedo, κ_i is the sea ice extinction coefficient (m^{-1}), h_i the ice thickness (m), $\kappa_B$is the is the spectral attenuation coefficient due to algae in the bottom ice (m^{-1}) and δ_z is the thickness of the algal layer (m^{-1}).

Assuming stable ice optical properties and negligible changes in basal absorption due to algal biomass, variability in transmittance can be attributed primarily to changes in snow depth and albedo. Such a simplification is motivated by the much higher optical extinction of snow relative to sea ice, meaning relatively small changes in snow thickness can strongly influence under-ice irradiance (Grenfell and Maykut, 1977; Fukami et al., 1985; Katlein et al., 2019). Under these assumptions, "Eq. (5)" reduces to an exponential dependence on snow thickness alone "Eq. (6)", using our measured transmittance:

$$\frac{T_2}{T_1} = \frac{(1-\alpha_s)e^{-\kappa_s h_2 - \kappa_i h_i - \kappa_B \delta_z}}{(1-\alpha_s)e^{-\kappa_s h_1 - \kappa_i h_i - \kappa_B \delta_z}} \quad (5)$$

$$\frac{T_2}{T_1} = e^{-\kappa_s (h_2 - h_1)} \quad (6)$$

Where T_2 is the transmittance where NCP becomes negative, T_1 is the measured transmittance, h_1 is the measured snow depth (m) and h_2 is the unknown snow depth (m).

While this approach neglects variability in ice optical properties and snow structure, it provides a useful framework for evaluating the influence of snow depth on under-ice light transmission and NCP estimates. Assuming a median literature snow attenuation coefficient of κ_s= 20 m^{-1} (Mundy et al., 2005; Perovich, 2007; Veyssière et al., 2022), we estimated the snow-depth threshold at which modelled NCP becomes negative. To do so, we first determined the reduction in PAR transmittance required to decrease the 24-hourly irradiance values used in the NCP calculations such that the resulting daily NCP equalled zero. This yielded a threshold transmittance (T_2). We then used "Eq. 6", together with T_1, h_1, and the assumed κ_s, to solve for the snow depth (h_2) required to produce T_2. Snow depths greater than h_2 were therefore predicted to result in negative daily NCP, allowing us to estimate the relative extent of net autotrophic and net heterotrophic conditions across the study region of the floe.

3. Results

3.1. Environmental conditions

The wind speed varied between approximately 2 to 18 m s^{-1} throughout the drift. Sustained winds over 15 m s^{-1} were observed from 25 May 1:00 lasting until 26 May 12:00 (Fig. 2). They meet the criteria of a storm (Cohen et

https://doi.org/10.5194/egusphere-2026-4031
Preprint. Discussion started: 15 July 2026

al., 2017) and accelerated the floe's southward drift, with speeds exceeding 0.53 m s^{-1}. From 19 May, the air temperatures increased from –6.8°C to near zero by 22 May (Fig. 2). Temperatures peaked at 3.9°C midday on 24 May before the storm system arrived (Fig. 2). Temperatures then began to drop, reaching a minimum of –10.5°C at the end of the storm period, when temperatures then began to increase again (Fig. 2).

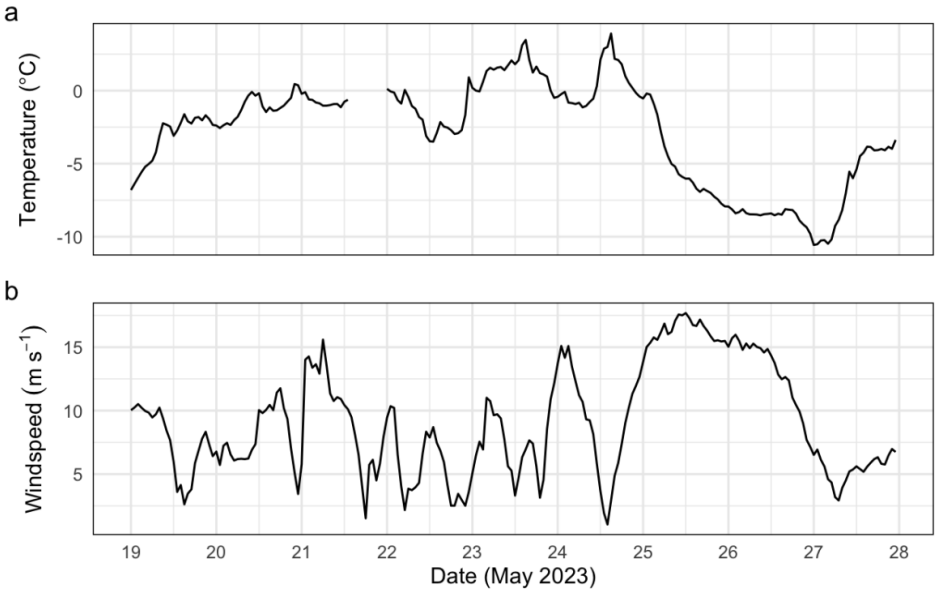

Figure 2: Hourly averaged atmospheric conditions measured above the ice during the sampling period including, (a) air temperature (°C) and (b) windspeed (m s^{-1}).

Hydrographic conditions varied among sampling sites, with differences in temperature and salinity observed within the upper 200 m of the water column (Fig. 3). At Sites 1 and 3, AW (T > 2°C; Sundfjord et al., 2020) occupied depths between approximately 100 and 200 m, and the mixed layer depth was 80 m. In contrast, Site 2 was characterized by a shallower mixed layer (30 m) and a warmer AW core, with temperatures reaching 2.8°C (Fig. 3).

https://doi.org/10.5194/egusphere-2026-4031
Preprint. Discussion started: 15 July 2026

385

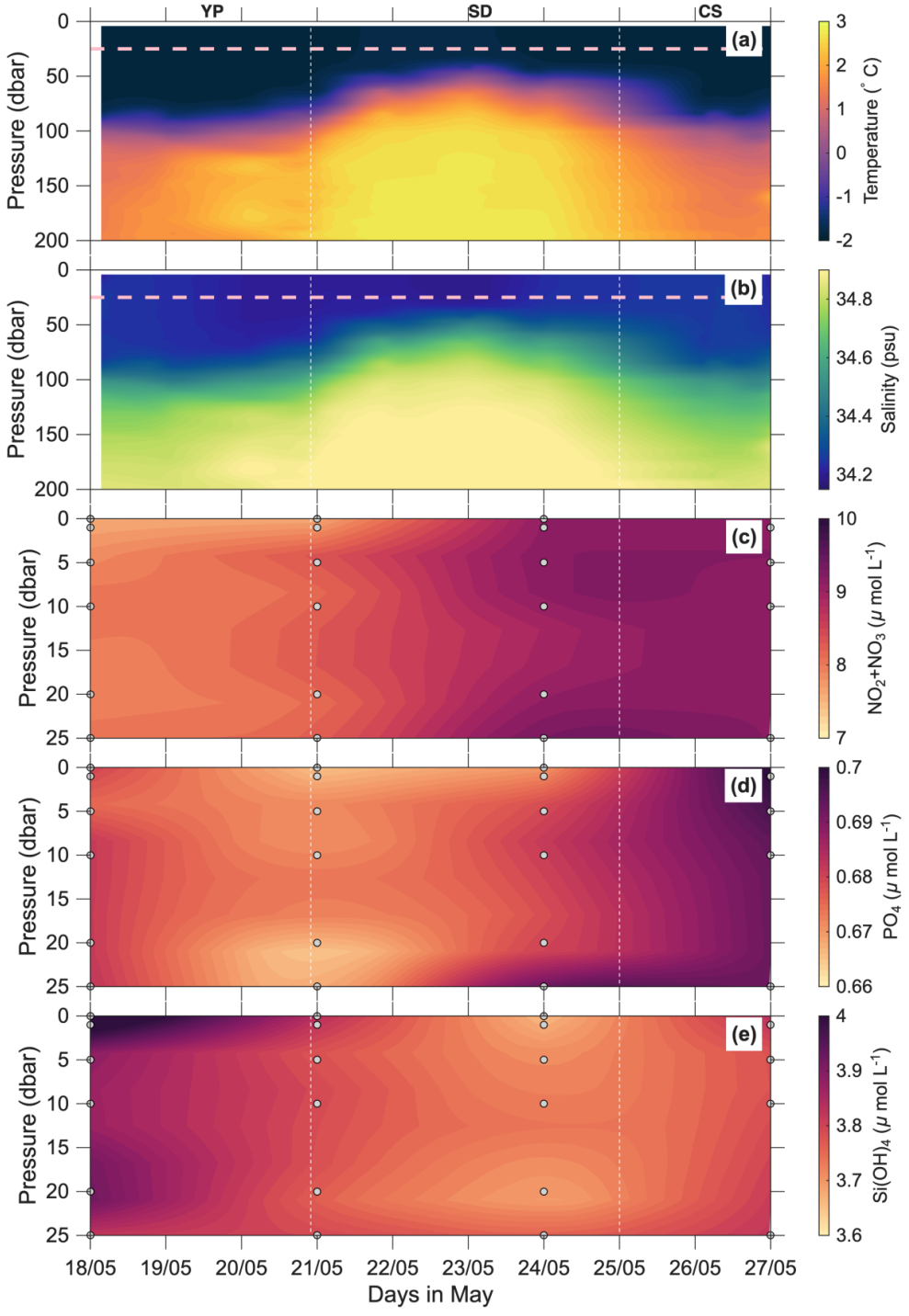

Figure 3: Hydrography of the upper water column over the duration of the study while located in the different

https://doi.org/10.5194/egusphere-2026-4031
Preprint. Discussion started: 15 July 2026

oceanographic regions of YP: Yermak plateau. SD: Sofia Deep. CS: Continental Slope, including: (a) Temperature and (b) Salinity, (c) Nitrate + nitrite (NO_3+NO_2), (d) Phosphate (PO_4) and (e) Silicic acid $Si(OH)_4$. Note that panels (c), (d) and (e) show the upper 25 m of the water column (indicated by the pink thick dashed line in panels (a) and (b)). The grey dots in panels c–e are the depths that water was collected at 0, 0.2, 1, 5, 10 and 25 m beneath the sea ice.

The nutrient concentrations in the water column varied throughout the drift (Fig. 3c–e), along with the differences in the origin of the AW. The under-ice water concentrations in the upper 25 m were 3.7–4.1 µmol L^{-1} and 7.4–9.5 µmol L^{-1} for $Si(OH)_4$ and NO_3+NO_2, respectively. Phosphate concentrations were between 0.6 to 0.7 µmol L^{-1}. Site 3 exhibited a significantly elevated NO_3+NO_2 concentration in the interface water relative to the other sites (Dixon's Q test, p = 0.04). Silicic acid decreased over sampling but not significantly while PO_4 interface water concentrations were not changing significantly (Dixon's Q test, $p > 0.05$).

The diapycnal diffusivity was enhanced in the upper 30 m of the water column and was at the noise level below that depth (not shown). The diapycnal diffusivity was significantly larger in the upper 25 m of the water column as the storm ended (around 10^{-2} m^{-2} s^{-1} on 26 May) before decreasing to values similar to the beginning of the drift (around 10^{-3} m^{-2} s^{-1} on 27 May; Fig. 4). The heat fluxes averaged in the upper 5 m of the water column were 2 W m^{-2} at the beginning and at the end of the drift, and 18 W m^{-2} as the storm ended (Fig. 4). The nitrate fluxes at the sea ice–ocean interface were larger right after the storm (0.15 mmol m^{-2} d^{-1}) and were close to zero otherwise (Fig. 4).

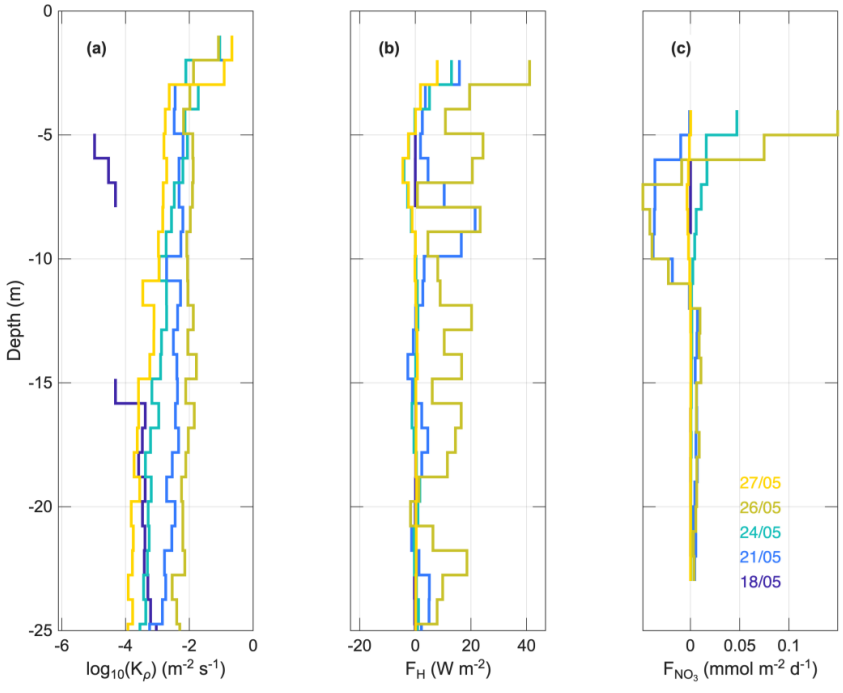

Figure 4: Vertical Profiles of Diapycnal Diffusivity K_ρ, Turbulent Heat Flux F_H, and Turbulent Nitrate Flux F_{NO_3}.

https://doi.org/10.5194/egusphere-2026-4031
Preprint. Discussion started: 15 July 2026

(a) Diapycnal diffusivity, (b) Vertical turbulent heat fluxes and (c) vertical nitrate (nitrate+nitrite) turbulent fluxes in the upper 25 m along the duration of the drift (18 May to 27 May, from dark blue to yellow). A storm event began early on 25 May and ended by mid-afternoon on 26 May.

The transects of the study region on the floe showed average snow depths from 0.17 ± 0.11 m to 0.31 ± 0.14 m over FYI, and 0.42 ± 0.17 m to 0.48 ± 0.20 m over SYI, with sea ice thickness ranging 1.75–2.05 m in FYI and 1.65–1.85 m in SYI (Table S1). It is likely the FYI area at the study floe formed in the beginning of the winter (October to January) in a refrozen lead (Fig. S1). Heavy snowfall occurred in the first half of the winter, resulting in differences in snow accumulation between SYI and FYI (Fig. S1). Additional snowfall in April/May, caused snow cover on both ice types to become similar through wind established equilibrium.

Based on the bulk salinity from the sea ice cores (Fig. S2), snow pits and transect data, we estimate that 70% of the research area on the floe consisted of SYI, while the remaining 30% was seasonal FYI formed from a frozen lead (Fig. S3). It was estimated that Site 1 ice samples were FYI, while Sites 2 and 3 were of SYI. The physical characteristics of the biogeochemical ice sampling sites of the floe are summarized in Table 2. Three sites were sampled for ice, with the comparison of two adjacent sites of differing snow depths at Site 2.

Table 2 Snow depth and ice thickness from biogeochemical ice coring, concentrations of particulate organic carbon and nutrients in the bottom–ice

Site / ice type	Snow depth (cm)	Ice thickness (cm)	POC (mg L^{-1})	PON (mg L^{-1})	$NO_3 + NO_2$ (µmol L^{-1})	PO4 (µmol L^{-1})	$Si(OH)_4$ (µmol L^{-1})
1 / FYI	9.1 ± 1.5	206.1 ± 1.8	5.73	0.85	3.57	0.84	1.00
2 / SYI	29.9 ± 0.9	130.7 ± 2.3	3.62	0.58	5.37	0.46	0.55
2 / SYI	17.3 ± 2.5	138.7 ± 2.2	2.72	0.43	3.21	0.46	0.97
3 / SYI	22.9 ± 2.1	143.9 ± 3.0	2.86	0.50	2.14	0.39	0.44

3.1. Algal abundance and taxonomy in the bottom–ice

Total photosynthetic cell abundance (flow cytometry) in the bottom ice was highest at Site 1 with approximately 90 $\times 10^3$ cells ml^{-1} and lowest at Site 3 with 36 $\times 10^3$ cells ml^{-1} (Fig. S7). The largest differences in abundance were observed in the nanoeukaryote size class, which ranged from 66 $\times 10^3$ cells ml^{-1} (Site 1) to 20 $\times 10^3$ cells ml^{-1} (Site 3). Abundances of microeukaryote (23 $\times 10^3$ cells ml^{-1} to 15 $\times 10^3$ cells ml^{-1}) and picoeukaryote (1.4 $\times 10^3$ cells ml^{-1} to 0.7 $\times 10^3$ cells ml^{-1}) were also observed to be lower between Sites 1 and 3 during sampling.

Based on light microscopy, the most common taxonomic group at all sites were pennate diatoms, contributing 58–73% of the microalgal community abundances (Text S1). Centric diatoms contributed consistently 12–13%, flagellates 9–23% (with the largest percentage being at the Site 2 thin snow), and dinoflagellates 3–7%. The most common genus was *Nitzschia spp*., with the colony forming *Nitzschia frigida*, making up 21–28% of the pennate community combined. *Pseudonitzschia spp*. was highly abundant (20% of the pennate diatom population) at Site 1 but contributed only 3–6% to the pennate community on other sampling dates.

https://doi.org/10.5194/egusphere-2026-4031
Preprint. Discussion started: 15 July 2026

3.2. Net community production (NCP) in the bottom–ice

The PI parameters derived from the NCP models are shown in Table 3. The average I_C was 2.68 ± 0.81 µmol photons m^{-2} s^{-1}, with all sites demonstrating photoinhibition (Fig. S8).

Table 3. Photosynthesis–irradiance (PI) parameters for bottom–ice incubations

Site / ice type	α^* (×10^{-3})	I_C	I_S	P_0^* (×10^{-2})	P_S^* (×10^{-2})	β^* (×10^{-4})	Daily integrated NCP	Chlorophyll *a* (mg m^{-2})
1 / FYI	1.80	2.86	7.28	0.452	1.31	0.66	0.74	7.07
2 / SYI thick snow	3.57	1.72	9.63	0.579	3.44	8.87	0.37	5.57
2 / SYI thin snow	2.13	3.67	10.04	0.700	2.14	6.42	–0.27	5.01
3 / SYI	5.47	2.48	11.55	1.252	6.31	3.31	3.21	3.93

α^*, photosynthetic efficiency (mol O_2 [g chl *a*]$^{-1}$ h^{-1} [µmol photons m^{-2} s^{-1}]$^{-1}$)
I_C, compensation irradiance (µmol photons m^{-2} s^{-1})
I_S, the photoacclimation parameter (µmol photons m^{-2} s^{-1})
P_0^*, production at zero irradiance (mol O_2 [g chl *a*]$^{-1}$ h^{-1})
P_S^*, maximum photosynthetic rate (mol O_2 [g chl *a*]$^{-1}$ h^{-1})
β^*, photoinhibition effect (mol O_2 [g chl *a*]$^{-1}$ h^{-1} [µmol photons m^{-2} s^{-1}]$^{-1}$)
NCP, net community production (mmol O_2 m^{-2} d^{-1})

Daily bottom-ice NCP, calculated from the PI parameters (Table 3) and hourly transmitted irradiances in the PAR range (Table S2 and Fig. S9), was highest at Site 3, with Site 2 showing the lowest estimates. The NCP was generally positive (i.e. net production of oxygen) except at Site 2 under thin snow where it was negative (indicating net consumption of oxygen).

3.3. Laboratory experiments relative to field incubations

Algal PI responses for the two cultured species were very similar (Table 4 and Fig. S10). The α^* (1.29 ± 0.33 ×10^{-3} mol O_2 [g chl *a*]$^{-1}$ h^{-1} [µmol photons m^{-2} s^{-1}]$^{-1}$) were lower than those of the bottom-ice communities, while the I_C (average 6.60 ±1.83 µmol photons m^{-2} s^{-1}) and I_S (22.13 ± 5.61 µmol photons m^{-2} s^{-1}) were higher (Tables 3 and 4). Values of P_S^* (2.77 ± 0.01 ×10^{-2} mol O_2 [g chl *a*]$^{-1}$ h^{-1}) and P_0^* (0.74 ± 0.02 ×10^{-2} mol O_2 [g chl *a*]$^{-1}$ h^{-1}) were intermediate to the bottom-ice values, being lower than Site 3 sampling (Tables 3 and 4).

Table 4. Photosynthesis–irradiance (PI) parameters for cultured incubations

Culture	α^* (×10^{-3})	I_C	I_S	P_0^* (×10^{-2})	P_S^* (×10^{-2})	β^* (×10^{-4})	Chlorophyll *a* (ug L^{-1})
Nitzschia frigida	1.06	7.89	26.09	0.753	2.76	0.71	79.8
Pseudonitzschia sp.	1.53	5.31	18.17	0.727	2.77	0.29	73.0

α^*, photosynthetic efficiency (mol O_2 [g chl *a*]$^{-1}$ h^{-1} [µmol photons m^{-2} s^{-1}]$^{-1}$)

https://doi.org/10.5194/egusphere-2026-4031
Preprint. Discussion started: 15 July 2026

I_C, compensation irradiance (µmol photons m^{-2} s^{-1})

I_S, the photoacclimation parameter (µmol photons m^{-2} s^{-1})

P_0^*, production at zero irradiance (mol O_2 [g chl a]$^{-1}$ h^{-1})

P_S^*, maximum photosynthetic rate (mol O_2 [g chl a]$^{-1}$ h^{-1})

β^*, photoinhibition effect (mol O_2 [g chl a]$^{-1}$ h^{-1} [µmol photons m^{-2} s^{-1}]$^{-1}$)

3.4. Floe-wide net community production estimate

Daily NCP was predicted to become negative when snow depth increased from 0.17 m to approximately 0.26 m, reducing transmittance from 2.56% to a critical threshold of 0.40%. This reduction lowered under-ice PAR irradiance from 7.03–22.3 to 1.10–3.49 µmol photons m^{-2} s^{-1}. Snow depth remained relatively constant over SYI but increased over FYI following the storm (Table S1). On 27 May, snow depths less than 0.30 m were observed predominantly over FYI, where mean snow depth was 0.31 ± 0.14 m, and FYI comprised approximately 30% of the study area (Sect. 3.1.). Applying the snow-depth threshold for negative NCP (0.26 m) to the observed snow distribution indicated that less than 1.1×10^5 m^2 of the study area could support net autotrophy, whereas approximately 2.5×10^5 m^2 was predicted to remain net heterotrophic.

4. Discussion: drivers of the variability in the algal community.

Throughout the drift, under-ice NO_3+NO_2 concentrations and transmitted irradiance varied, both of which are important controls on sea-ice algal production (Castellani et al., 2017; Leu et al., 2015). As NO_3+NO_2 availability and irradiance varied over time, we observed changes in the magnitude of chl a concentration and NCP, driven by the combined influence of these environmental factors. In addition, the occurrence of a storm introduced further changes, modifying conditions of the ice floe and underlying water column. Here, we examine the individual roles of changing sub-ice nutrient dynamics, shifting light regimes, and the impact of the storm event forcing in shaping the observed patterns of ice algal biomass and production.

4.1. Nutrient dynamics under the ice

Nutrient conditions for ice algae and phytoplankton in the Arctic Ocean are often considered limiting due to stratification and supply of nutrients relative to biological demands (Bluhm et al., 2015; Ahmed et al., 2025). The continental slope and adjacent Yermak Plateau region north of Svalbard have the potential for enhanced primary production due to the proximity of nutrient-rich North Atlantic surface waters, which stimulate the growth of both ice algae and phytoplankton (Assmy et al., 2017; Ehrlich et al., 2021). In addition, the nearby continental shelves may serve as a source of algal cells, facilitating their transport and colonization of sea ice in the region (Oziel et al., 2020). However, upward heat flux from AW, particularly in open and semi-open ocean regions, contributes to sea-ice melt in both the Eurasian Basin and the Barents Sea (Duarte et al., 2020). This influence is expected to intensify in the coming years due to ongoing Atlantification of the Eurasian Basin and global warming (Ingvaldsen et al., 2021).

We observed differences in NO_3+NO_2 but consistent PO_4 and an insignificant decrease in $Si(OH)_4$ concentrations in the upper 25 m of the Polar Surface Water as the study floe first drifted north-eastward and then

https://doi.org/10.5194/egusphere-2026-4031
Preprint. Discussion started: 15 July 2026

south-westward (Fig. 3). These observations suggest that differences in nutrient concentrations within the Polar Surface Water were influenced by the nutrient characteristics of the underlying AW, which were transmitted upward through vertical mixing. Differences in concentrations may be a result of known differences in the NO_3+NO_2 concentration between different branches of the underlying Atlantic waters as they flow north of Svalbard (Koenig 2021). Here, the Yermak Pass Branch and the Yermak Branch (Site 1) featured the lowest NO_3+NO_2 concentrations in the upper 25 m. Site 2 (Sofia Deep) was more influenced by water from the Atlantic Water Boundary Current, with NO_3+NO_2 concentrations intermediate between the Yermak and Svalbard branches, reflecting mixing between these two sources. Site 3 was enriched in NO_3+NO_2 compared to the other sites (Dixon's Q test, $p = 0.04$), it was influenced by the Svalbard Branch, which originates from west of Svalbard and is younger than the water found over the Yermak Plateau (Fig. 1a; Koenig et al., 2017; Meyer et al., 2017a).

Although nitrate is often considered the primary limiting nutrient for phytoplankton growth in AW (Krisch et al., 2020), there was evidence of $Si(OH)_4$ limitation in our study, consistent with previous findings (Duarte 2021; Renner, 2023). Relative to expected stoichiometric Redfield ratios (Brzezinski, 1985), N:Si ratios in the sea ice and under-ice water of this study were elevated, and Si:P ratios were lower. Given the bottom ice consistently exhibited higher N:Si and lower Si:P ratios than the underlying water column (Table S3), it is likely that Si depletion within the ice was due to biological incorporation into the frustules of diatoms, which were the dominant taxonomic group (Text S1). Consistent with these ratios, bottom-ice nutrient concentrations normalized to interface-water salinity showed $Si(OH)_4$ depletion, except at the thin-snow site (Table S3). Variability in AW influence likely contributed to these patterns, with high N:Si and low N:P ratios indicating potential co-limitation by nitrogen and silicate (Table S3) (Krause et al., 2018; Vonnahme et al., 2021).

Despite indications of potential $Si(OH)_4$ limitation across all sites, we found little evidence that variability in $Si(OH)_4$ availability explained differences in productivity. Although Site 1 exhibited the highest interface-water $Si(OH)_4$ concentrations, $Si(OH)_4$ concentrations differed little among sites. However, Site 1 was distinguished by the lowest NO_3+NO_2 concentrations, highest POC:PON molar ratio (7.91), and the lowest P_S^*. Together, these observations indicate lower productivity and reduced incorporation of organic nitrogen at the time of sampling. In contrast, Site 3 exhibited higher NO_3+NO_2 interface water concentrations, coinciding with lower POC:PON ratios (6.67) and elevated P_S^*, suggesting that nitrogen was not limiting at this site and a stronger influence of nitrogen availability on productivity (Geider & La Roche, 2002). This interpretation is further supported by salinity-normalized bottom ice nutrient concentrations indicating enrichment of NO_3+NO_2 in the bottom ice relative to expected stoichiometric relationships with $Si(OH)_4$. Previous studies have shown that diatoms can reduce their cellular silica requirements under elevated environmental N:Si ratios, thereby alleviating $Si(OH)_4$ limitation (McNair et al., 2018). Increased NO_3+NO_2 availability may facilitate this response by supporting the protein requirements of silicic acid transport systems (Durkin et al., 2013), and reduced $Si(OH)_4$ availability does not necessarily constrain phytoplankton growth (Thielecke et al., 2026). Collectively, these observations suggest that NO_3+NO_2 availability exerted a stronger influence on productivity than $Si(OH)_4$ availability during our study.

https://doi.org/10.5194/egusphere-2026-4031
Preprint. Discussion started: 15 July 2026

4.2. The changing light environment of bottom ice communities of first year- and second year ice

Chlorophyll *a* concentrations in the present study (75–130 µg L^{-1}) were approximately one to two orders of magnitude higher than previously reported values (<0.5 – 9 µg L^{-1}) in April-June for the region (Kowalczuk et al., 2017; Olsen et al., 2017; Ehrlich et al., 2020). However, part of this difference likely reflects methodological variation among studies. Kowalczuk et al. (2017) integrated chl *a* over the bottom 20 cm of the ice, while Ehrlich et al. (2020) and Olsen et al. (2017) sampled the bottom 10 cm of SYI. In contrast, our measurements were restricted to the bottom 5 cm of both FYI and SYI. Nevertheless, the substantially higher concentrations observed here suggest considerable interannual variability in ice algal biomass.

The study floe consisted of older SYI with a snow cover that was, on average, approximately 0.2 m thicker compared to FYI locations. Given the strong negative relationship between ice–snow thickness and light transmission (Nicolaus et al., 2013), the differences in ice thickness and snow cover associated with ice age across our floe would have drove variability in light environment that is likely reflected by the variability in bottom-ice chl *a*. Here, the highest chl *a* (7 mg m^{-2}) was in the bottom of FYI sampled under 0.09 m of snow at Site 1, while values were 10–43% lower at the SYI Sites 2 and 3, which had thicker snow covers of about 0.17 to 0.30 m.

We also observed variability in the community composition amongst sites/ice ages, though pennate diatoms dominated all bottom-ice communities (Supp. Text 1). The FYI site contained a greater abundance of nanoeukaryotes, primarily small pennate diatoms, than the SYI sites (Supp. Text S1). The community composition of Site 1 (FYI) had a higher proportion of *Pseudonitzschia spp.* compared to the other sites where *N. frigida* was more abundant. This difference may have driven NCP variability between sampling sites (Rochet et al., 1986; Campbell et al., 2022). However, in our laboratory experiments of *Pseudonitzschia* spp. versus *N. frigida*, their PI responses were nearly identical under the same growing conditions (Table 4), and as a result, species variability was unlikely to be the main driver of NCP variability between these sample sites.

Bottom ice communities in the northern Barents Sea and coastal Arctic are often dominated by *Nitzschia frigida* (Lewis et al., 2026), comprising more than 75% of total cell abundance in ice thicker than 120 cm and showing a significant positive association with snow depth (Hegseth & von Quillfeldt, 2022). In contrast, other diatom taxa may become dominant under conditions of greater light availability and nutrient supply (Hegseth & von Quillfeldt, 2022). This suggests that species differ in their environmental optima and that shifts in community composition may reflect changes in competitive advantage under varying environmental conditions (Croteau et al., 2021; Croteau et al., 2022). The similar physiological responses observed in our nutrient-replete monoculture experiments indicate that species turnover within the diatoms may have limited consequences for NCP when environmental conditions select for the most competitive species. We suggest that variability between taxonomic groups (i.e. especially between different snow covers at Site 2) was likely important for the magnitude of NCP, whereas variability within a taxonomic group (i.e. between species) was not.

4.2.1. Net community production due to light availability

Sampling of two adjacent snow covers (thick and thin) over SYI at Site 2 highlights the spatial variability in both the magnitude of NCP across the study floe. Although under-ice water NO_3+NO_2 concentrations were higher than at Site 1, NCP was lower, suggesting that nutrient availability was not the only factor limiting production at this site. Instead, the thick snow cover, low downwelling irradiance on the sampling date, and accumulation of

https://doi.org/10.5194/egusphere-2026-4031
Preprint. Discussion started: 15 July 2026

NO_3+NO_2 in the bottom ice suggest that the bloom was at an earlier stage of development and had not yet progressed to nutrient limitation (Fripiat et al., 2017; Henley et al., 2020). The relatively elevated NO_3+NO_2 concentrations in the bottom ice beneath the thicker snow cover may also reflect enhanced nitrification under low-light conditions (Shiozaki et al., 2019; Clark et al., 2020), or intracellular nutrient storage (Mundy et al., 2025).

In contrast, NCP was negative beneath the thinner snow cover despite greater light availability. We hypothesize that the community composition at this site could have been a factor in driving the net heterotrophic conditions. Here, we documented a higher relative abundance of flagellate cells (Supp. Text S1), which are typically comprised of heterotrophic and/or mixotrophic taxa. This scenario is further supported by the thin-snow site being the only location where salinity-normalized bottom-ice $Si(OH)_4$ concentrations exceeded those of the ice–water interface (Table S3), potentially suggesting limited uptake of this diatom-associated nutrient. Additionally, incident irradiance on the sampling date was more than 30% lower than during previous sampling periods because of heavy cloud cover, which further reduced the calculated daily integrated NCP. These observations highlight how variability in community composition and snow cover may collectively influence sea-ice NCP.

4.2.2. Photoacclimation under variable snow cover

Due to the inherent variability in sea ice algal PI parameters (Barlow et al., 1988; Kvernvik et al., 2021), and our limited sampling of three locations, it is challenging to draw conclusions on the drivers of spatiotemporal variability in algal photophysiology. However, we do find examples of PI responses that likely represent light acclimation. The thinnest snow cover was at Site 1, corresponding to the lowest α^* (Table 3), which is characteristic of algal photoacclimation to increasing light intensities (Cota, 1985; Wolf et al., 2022). Photoinhibition was also lowest at this site, indicating a tolerance of comparatively high light exposure (Lund-Hansen et al., 2020). These findings were further corroborated by the relatively high–light acclimated laboratory culture incubations, which were initially grown at 30 µmol photons m^{-2} s^{-1}, and produced similar α^* and β values.

4.3 Short-term drivers of bottom-ice communities: Storms

The storm event on 25–26 May represented a period of intense short-term forcing that altered both the physical and biological conditions at the ice–ocean interface. Enhanced water-column mixing during the storm, reflected by elevated diapycnal diffusivity (Fig. 5), increased upward nutrient fluxes into the bottom ice and likely enhanced nutrient availability for bottom-ice algal communities. In particular, the large flux of NO_3+NO_2 into the ice on 26 May suggests that the storm was an important driver of nutrient supply to the bottom ice. While increased NO_3+NO_2 availability at Site 3 reflected the influence of the underlying Svalbard Branch of AW on the overlying surface waters (Sect. 4.1), storm-driven mixing associated with the rapid southward drift of the floe likely reinforced this nutrient enrichment on short timescales.

Evidence for a biological response to the enhanced nutrient supply at Site 3 is evidenced by greater NCP here than at the other Site (Table 3). The combination of elevated water-column NO_3+NO_2 concentrations and increased nutrient flux during the storm likely contributed to this enhanced production, consistent with modelling studies highlighting the importance of turbulent nutrient supply for sustaining ice algal production (Duarte et al., 2022). When converted to carbon units, daily net community production at Site 3 reached 46.3 mg C m^{-2} d^{-1},

https://doi.org/10.5194/egusphere-2026-4031
Preprint. Discussion started: 15 July 2026

exceeding the highest previously reported primary production rates from this region (34.5 mg C m^{-2} d^{-1}; Ehrlich et al., 2021). The higher values of a^*, I_S, and P_S^* at Site 3 further support the influence of greater nutrient availability, as these photophysiological parameters are known to increase under nutrient-replete conditions (Campbell et al., 2016).

At the same time, the storm likely contributed to the loss of algal biomass from the bottom ice. Prior to the storm, above-freezing air temperatures and a warming snowpack (Fig. S5) had produced a nearly isothermal ice column at Site 3 (Fig. S2), with visual evidence of bottom ice melt (pers. Comm. P. Itkin). Storm-driven heat fluxes into the ice (Fig. 5) would have further weakened the skeletal layer and promoted basal melt. This interpretation is supported by the simultaneous occurrence of elevated productivity and lower algal biomass (Table 3), a pattern previously observed during periods of bottom ice deterioration when active production continues despite ongoing biomass loss (Demers et al., 1989; Rysgaard et al., 2001; Lavoie et al., 2005). Although the relative contributions of basal melt, brine drainage, and turbulent mixing cannot be distinguished here, each of these processes can increase the connectivity of the ice matrix or physically dislodge cells from the ice, thereby facilitating the release of sea-ice algae to the underlying water column. Such release is recognized as an important source of carbon export in the region (Dybwad et al., 2022).

The storm also modified snow conditions. Snow accumulation increased on FYI while remaining relatively unchanged on SYI (Table S1), consistent with storm-driven snow redistribution processes (Mallett et al., 2022). Following the event, snow depths became more uniform across the floe, reducing light availability over FYI. Concurrently, FYI experienced a decrease in ice thickness whereas SYI thickness remained relatively stable, indicating enhanced basal melt of FYI (Table S1). The higher salinity of FYI lowers its melting point, while thinner snow cover provides less insulation (Merkouriadi et al., 2020), likely increasing its susceptibility to melt. These effects made the initially higher algal biomass in FYI particularly vulnerable to loss during the period of elevated heat flux. Together, these observations suggest that spring storms can simultaneously enhance nutrient supply and productivity while accelerating biomass loss through warming, melt, and physical disruption, with potentially stronger impacts on FYI than SYI.

4.3. Floe-wide NCP estimate

Despite the temporal and spatial heterogeneity in sea-ice NCP observed across our study floe, it remains necessary to estimate production at larger spatial scales. Because the under-ice light field is highly heterogeneous (Lange et al., 2016), spatially averaged PAR measurements provide a more representative characterization of light availability than individual point measurements (Matthes et al., 2020). We therefore used the observed snow-depth averages to upscale our auto- heterotrophy threshold analysis across the floe, as snow thickness controls under-ice irradiance and thus whether bottom-ice communities are predicted to be net autotrophic or net heterotrophic. Applying the calculated critical snow-depth threshold of 0.26 m suggested that net autotrophy was likely concentrated in FYI regions, whereas much of the SYI area remained net heterotrophic (Table S1). We estimated floe-wide NCP during a period of relatively higher observed downwelling irradiance and following elevated nitrate flux into the ice, conditions that were relatively favourable for sea-ice algal productivity. Although we acknowledge that rates may vary with community composition and local environmental conditions across the floe, based on this approach, we estimate that the study region was likely net heterotrophic during sampling.

https://doi.org/10.5194/egusphere-2026-4031
Preprint. Discussion started: 15 July 2026

Though estimates of snow depth across the Arctic are limited, average April snow depths have been estimated at approximately 17 cm on FYI and 27 cm on SYI (Kwok et al., 2020). These values are consistent with our observations of thinner FYI snow covers, indicating that autotrophic light conditions are more likely to occur under FYI. During our study, snow thickness remained relatively unchanged on SYI, whereas storm-driven redistribution increased snow accumulation on FYI. Snow redistribution acts to equilibrate snow cover between adjacent ice, particularly in rough SYI where snow thickness is highly variable (Mallett et al., 2022). Because snow depth strongly regulates light transmission through sea ice, these redistribution events can alter NCP by shifting the balance between photosynthesis and respiration.

Recent studies highlight that sea-ice ecosystems can remain net heterotrophic under a range of environmental conditions. Campbell et al. (2022) reported consistently heterotrophic conditions across both FYI and multiyear ice floes, whereas McKay et al. (2026) found that regional patterns of autotrophy and heterotrophy depended strongly on sub-ice mixing. Our observations further emphasize that algal biomass may continue to accumulate even when community respiration exceeds gross photosynthetic production, indicating a decoupling between algal growth and net community metabolic balance. Such conditions may arise when heterotrophic respiration is supported by previously produced or allochthonous organic matter (Dezutter et al., 2020; Raymond & Bauer, 2001), or when short-term measurements capture transient periods of net heterotrophy within a broader interval of positive algal growth (del Giorgio et al., 2005).

5. Conclusions

We observed distinct nutrient regimes within the water column as our study floe drifted, with corresponding impacts on NCP in bottom-ice communities. In cases of Si–N co-limitation, nitrate availability may exert a greater control on productivity and photoacclimation. These findings highlight the importance of nutrient fluxes, rather than nutrient concentrations alone, in regulating sea-ice productivity, with enhanced nitrogen delivery potentially supporting increased production. Changes in the light environment further influenced chl *a* accumulation and the balance between heterotrophic and autotrophic processes across different ice ages. Even when nutrient concentrations are high, rapid environmental changes such as cloud cover can shift NCP towards heterotrophy. Given the complexity of the natural sea-ice environment, it remains challenging to disentangle the relative importance of these interacting drivers on algal community dynamics. However, this dataset provides an excellent foundation for future modelling efforts aimed at identifying the primary controls on the system.

Our results demonstrate that sea-ice NCP is highly dynamic and spatially heterogeneous at the floe scale in spring. The findings of this study also underscore the influence of upward nutrient and heat fluxes on sea ice in the region north of Svalbard. The high rate of NCP observed during the storm event, which exceeded the limited previous productivity estimates available for the region, suggest that episodic mixing events may contribute substantially to sea-ice production. Determining the frequency and spatial extent of such storm-enhanced production will be critical for assessing its contribution to regional sea-ice productivity and whether these processes may become increasingly important farther into the Eurasian Basin as Atlantification strengthens. While increased oceanic exchange can enhance nutrient delivery to bottom-ice algae, the associated heat fluxes may promote basal melt and reduce overall sea-ice community size, underscoring the potentially contradictory effects of mixing on sea-ice ecosystem productivity (Campbell et al., 2014; Renner et al., 2023).

https://doi.org/10.5194/egusphere-2026-4031
Preprint. Discussion started: 15 July 2026

Although the storm supplied additional nutrients to the sea ice, widespread heterotrophy persisted within the bottom ice due to light limitation. Our results show that even mid spring, heavy drifting snow can limit sea-ice algal production by reducing light to levels that drive oxygen consumption (net negative NCP). As open water and FYI increase with climate change, enhanced turbulence is expected alongside reductions in sea ice thickness and changes in snow cover (Lannuzel et al., 2020; Timmermans and Marshall, 2020; Chen et al., 2024). These competing processes are likely to widen the knowledge gap in sea ice NCP, with the potential to enhance NCP through increased nutrient supply and light availability, while also reducing it via increased snowfall, a reduction in seeding from older ice, habitat loss and melt–associated processes.

Code availability

The R and MATLAB code used for analyses are available from the corresponding author upon request.

Data availability

Data have been published at the Norwegian Polar Data Centre under the following:
McKay, R., Osanen, J., Laber, C., and Campbell, K.: Sea ice biogeochemical data for the BREATHE project: Yermak Plateau 2023 [Dataset], Norwegian Polar Institute, https://doi.org/10.21334/NPOLAR.2025.18D7E643, 2025.

Itkin, P.: Sea ice core data from BREATHE/SIDRiFT field school, north of Svalbard, May 2023 [Dataset], Norwegian Polar Institute, https://doi.org/10.21334/NPOLAR.2025.44A880E0, 2025.

Itkin, P., Snow pits from BREATHE/SIDRiFT field school, north of Svalbard, May 2023 [Dataset], Norwegian Polar Institute, https://doi.org/10.21334/NPOLAR.2024.A1AB4151, 2025.

Koenig, Z. and Campbell, K.: Microstructure Profiler (MSS) profiles from the BREATHE project: Yermak Plateau 2023 [Dataset], Norwegian Polar Institute, https://doi.org/10.21334/NPOLAR.2026.05015061, 2026.

A more detailed report of the fieldwork is available in the at the Norwegian Polar Data Centre under the following: Campbell, K., Itkin, P., McKay, R., Osanen, J., Gätcher, M., and Koenig, Z.: Cruise Report for the BREATHE project: Yermak Plateau 2023 [Dataset], Norwegian Polar Institute, https://doi.org/10.21334/NPOLAR.2025.DF42A46F, 2025.

Supplement

This research includes supplementary material (Tables S1 to S3, Figures S1 to S10 and Text S1) that have been uploaded separately to this document.

https://doi.org/10.5194/egusphere-2026-4031
Preprint. Discussion started: 15 July 2026

Author Contributions

- Contributed to conception and design: RDM, KC, ZK
- Contributed to acquisition of data: RDM, JO, PI, ZK, CL, KC
- Contributed to analysis and interpretation of data: RDM, ZK, RG, PI, SSH, KC
- Drafted and/or revised the article: RDM, ZK, RG, CL, JO, KC
- Approved the submitted version for publication: RDM, ZK, RG, SSH, PI, CL, JO, KC

Competing interests

The authors declare that they have no conflict of interest.

Acknowledgements

We would like to thank the students of the BREATHE (Bottom-sea ice Respiration and nutrient Exchanges Assessed for THE Arctic) and SiDRIFT (Sea Ice Deformation and Snow for an Arctic in Transition) sea ice school for their contributions to collecting samples for this work. We thank the captain, officers, and crew of RV *Kronprins Haakon* for their professionalism, patience, and support throughout the expedition and the associated PhD school. Also a big thank you to Reidar Kaasa (UiT) for his technical help with equipment and sensors.

Financial support

This work is a part of the BREATHE research project funded by the Research Council of Norway (Project number 325405), and is a contribution to the Micro-SHIFT (Microbial life in Sea ice Habitats Investigated for The Arctic) ERC StG of K Campbell (no. 101162830). P.I. acknowledges funding from the Research Council of Norway project SiDRIFT (Project number 287871). Z.K. acknowledges funding from the Research Council of Norway (Project number 352217) DIAMOND (Sea Ice Lead Dynamics in the Arctic and their impact on primary production).

References

Aagaard, K., Coachman, L. K., and Carmack, E.: On the halocline of the Arctic Ocean, Deep-Sea Res., 28, 529–545, https://doi.org/10.1016/0198-0149(81)90115-1, 1981.

Ahmed, F., Leu, E., Juhl, A. R., Campbell, K., Dilliplaine, K. B., Assmy, P., Niemi, A., Gradinger, R., Alou-Font, E., Torres-Valdés, S., Whitmore, L., Jones, E. M., Fransson, A., Chierici, M., Olsen, L. M., McKay, R. D., Lee, S. H., Oggier, M., Lange, B. A., Tremblay, J. É., Gosselin, M., and Mundy, C. J.: A pan-Arctic perspective on the influence of ice algae on sea-ice nutrient concentrations, Elem. Sci. Anthr., 13, 00059, https://doi.org/10.1525/elementa.2025.00059, 2025.

Andersen, R. A. (Ed.): Algal Culturing Techniques, Elsevier Academic Press, New York, 578 pp., 2005.

https://doi.org/10.5194/egusphere-2026-4031
Preprint. Discussion started: 15 July 2026

Anderson, L. G., Andersson, P. S., Björk, G., Jones, E. P., Jutterström, S., and Wåhlström, I.: Source and formation of the upper halocline of the Arctic Ocean, J. Geophys. Res. Oceans, 118, 410–421, https://doi.org/10.1029/2012JC008291, 2013.

Arrigo, K. R., Mills, M. M., Kropuenske, L. R., Van Dijken, G. L., Alderkamp, A. C., and Robinson, D. H.: Photophysiology in two major Southern Ocean phytoplankton taxa: photosynthesis and growth of *Phaeocystis antarctica* and *Fragilariopsis cylindrus* under different irradiance levels, *Integr. Comp. Biol.*, 50(6), 950–966, https://doi.org/10.1093/icb/icq021, 2010.

Assmy, P., Ehn, J. K., Fernández-Méndez, M., Hop, H., Katlein, C., Sundfjord, A., Bluhm, K., Daase, M., Engel, A., Fransson, A., Granskog, M. A., Hudson, S. R., Kristiansen, S., Nicolaus, M., Peeken, I., Renner, A. H. H., Spreen, G., Tatarek, A., and Wiktor, J.: Floating ice-algal aggregates below melting Arctic sea ice, PLoS ONE, 8, e76599, https://doi.org/10.1371/journal.pone.0076599, 2013.

Assmy, P., Fernández-Méndez, M., Duarte, P., Meyer, A., Randelhoff, A., Mundy, C. J., Olsen, L. M., Kauko, H. M., Bailey, A., Chierici, M., et al.: Leads in Arctic pack ice enable early phytoplankton blooms below snow-covered sea ice, Sci. Rep., 7, 40850, https://doi.org/10.1038/srep40850, 2017.

Bagshaw, E. A., Wadham, J. L., Mowlem, M., Tranter, M., Eveness, J., Fountain, A. G., and Telling, J.: Determination of dissolved oxygen in the cryosphere: a comprehensive laboratory and field evaluation of fiber optic sensors, Environ. Sci. Technol., 45, 700–705, https://doi.org/10.1021/es102571j, 2011.

Barlow, R. G., Gosselin, M., Legendre, L., Therriault, J.-C., Demers, S., Mantoura, R. F. C., and Llewellyn, C. A.: Photoadaptive strategies in sea-ice microalgae, Mar. Ecol. Prog. Ser., 45, 145–152, https://doi.org/10.3354/meps045145, 1988.

Bluhm, B. A., Kosobokova, K. N., and Carmack, E. C.: A tale of two basins: an integrated physical and biological perspective of the deep Arctic Ocean, Prog. Oceanogr., 139, 89–121, https://doi.org/10.1016/j.pocean.2015.07.011, 2015.

Brzezinski, M. A.: The Si:C:N ratios of marine diatoms: interspecific variability and the effect of some environmental variables, J. Phycol., 21, 345–357, https://doi.org/10.1111/j.0022-3646.1985.00347.x, 1985.

Campbell, K., Lange, B. A., Landy, J. C., Katlein, C., Nicolaus, M., Anhaus, P., Matero, I., Gradinger, R., Charette, J., Duerksen, S., Tremblay, P., Rysgaard, S., Tranter, M., Haas, C., and Michel, C.: Net heterotrophy in High Arctic first-year and multi-year spring sea ice, Elem. Sci. Anthr., 10, 00040, https://doi.org/10.1525/elementa.2021.00040, 2022.

Campbell, K., Mundy, C. J., Barber, D. G., and Gosselin, M.: Remote estimates of ice algae biomass and their response to environmental conditions during spring melt, Arctic, 67, 375–387, https://doi.org/10.14430/arctic4409, 2014.

Campbell, K., Mundy, C. J., Landy, J. C., Delaforge, A., Michel, C., and Rysgaard, S.: Community dynamics of bottom-ice algae in Dease Strait of the Canadian Arctic, Prog. Oceanogr., 149, 27–39, https://doi.org/10.1016/j.pocean.2016.10.005, 2016.

Campbell, K., Mundy, C. J., Belzile, C., Delaforge, A., and Rysgaard, S.: Seasonal dynamics of algal and bacterial communities in Arctic sea ice under variable snow cover, Polar Biol., 41, 41–58, https://doi.org/10.1007/s00300-017-2168-2, 2018.

https://doi.org/10.5194/egusphere-2026-4031
Preprint. Discussion started: 15 July 2026

Campbell, K., Mundy, C. J., Juhl, A. R., Dalman, L. A., Michel, C., Galley, R. J., Else, B. E., Geilfus, N. X., and Rysgaard, S.: Melt procedure affects the photosynthetic response of sea ice algae, Front. Earth Sci., 7, 21, https://doi.org/10.3389/feart.2019.00021, 2019.

Castellani, G., Losch, M., Lange, B. A., and Flores, H.: Modeling Arctic sea-ice algae: physical drivers of spatial distribution and algae phenology, *J. Geophys. Res. Oceans*, 122(9), 7466–7487, https://doi.org/10.1002/2017JC012828, 2017.

Castellani, G., Veyssière, G., Karcher, M., Stroeve, J., Banas, S. N., Bouman, A. H., Brierley, S. A., Connan, S., Cottier, F., Große, F., Hobbs, L., Katlein, C., Light, B., McKee, D., Orkney, A., Proud, R., and Schourup-Kristensen, V.: Shine a light: under-ice light and its ecological implications in a changing Arctic Ocean, Ambio, 51, 307–317, https://doi.org/10.1007/s13280-021-01662-3, 2022.

Castellani, G., Campbell, K., Moreau, S., and Duarte, P.: Turbulence-Driven Nutrient Supply Sustains Algal Growth in the Arctic: A Modeling Approach, EGUsphere [preprint], https://doi.org/10.5194/egusphere-2025-5384, 2026.

Castro de la Guardia, L., Garcia-Quintana, Y., Claret, M., Hu, X., Galbraith, E. D., and Myers, P. G.: Assessing the role of high-frequency winds and sea ice loss on Arctic phytoplankton blooms in an ice–ocean–biogeochemical model, J. Geophys. Res.-Biogeo., 124, 2728–2750, https://doi.org/10.1029/2018JG004869, 2019.

Cauwet, G.: Determination of dissolved organic carbon and nitrogen by high temperature combustion, in: Methods of Seawater Analysis, John Wiley & Sons, 407–420, https://doi.org/10.1002/9783527613984.ch15, 1999.

Cavallo, S. M., Frank, M. C., and Bitz, C. M.: Sea ice loss in association with Arctic cyclones, Commun. Earth Environ., 6, 44, https://doi.org/10.1038/s43247-025-02022-9, 2025.

Chen, S., Liu, J., Song, M., Inoue, J., and Ding, Y.: An intercomparison of snow mass budget over Arctic sea ice simulated by CMIP6 models, J. Climate, 37, 2119–2139, https://doi.org/10.1175/JCLI-D-22-0539.1, 2024.

Clark, S. C., Granger, J., Mastorakis, A., Aguilar-Islas, A., and Hastings, M. G.: An investigation into the origin of nitrate in Arctic sea ice, Global Biogeochem. Cycles, 34, e2019GB006279, https://doi.org/10.1029/2019GB006279, 2020.

Cohen, L., Hudson, S. R., Walden, V. P., Graham, R. M., and Granskog, M. A.: Meteorological conditions in a thinner Arctic sea ice regime from winter to summer during the Norwegian Young Sea Ice expedition (N-ICE2015), J. Geophys. Res.-Atmos., 122, 7235–7259, https://doi.org/10.1002/2016JD026034, 2017.

Cota, G. F.: Photoadaptation of high Arctic ice algae, Nature, 315, 219–222, https://doi.org/10.1038/315219a0, 1985.

Crawford, A. D., Lukovich, J. V., McCrystall, M. R., Stroeve, J. C., and Barber, D. G.: Reduced sea ice enhances intensification of winter storms over the Arctic Ocean, J. Climate, 35, 3353–3370, https://doi.org/10.1175/JCLI-D-21-0747.1, 2022.

Crews, L., Sundfjord, A., and Hattermann, T.: How the Yermak Pass branch regulates Atlantic water inflow to the Arctic Ocean, J. Geophys. Res. Oceans, 124, 267–280, https://doi.org/10.1029/2018JC014476, 2019.

https://doi.org/10.5194/egusphere-2026-4031
Preprint. Discussion started: 15 July 2026

Croteau, D., Guérin, S., Bruyant, F., Ferland, J., Campbell, D. A., Babin, M., and Lavaud, J.: Contrasting nonphotochemical quenching patterns under high light and darkness aligns with light niche occupancy in Arctic diatoms, Limnol. Oceanogr., 66, S231–S245, https://doi.org/10.1002/lno.11587, 2021.

Croteau, D., Lacour, T., Schiffrine, N., Morin, P. I., Forget, M. H., Bruyant, F., Ferland, J., Lafond, A., Campbell, D. A., Tremblay, J. É., Babin, M., and Lavaud, J.: Shifts in growth light optima among diatom species support their succession during the spring bloom in the Arctic, J. Ecol., 110, 1356–1375, https://doi.org/10.1111/1365-2745.13874, 2022.

Dalman, L. A., Else, B. G. T., Barber, D., Carmack, E., Williams, W. J., Campbell, K., Duke, P. J., Kirillov, S., and Mundy, C. J.: Enhanced bottom-ice algal biomass across a tidal strait in the Kitikmeot Sea of the Canadian Arctic, *Elem. Sci. Anth.*, 7(22), https://doi.org/10.1525/elementa.361, 2019.

del Giorgio, P. A. and Williams, P. J. le B.: The global significance of respiration in aquatic ecosystems: from single cells to the biosphere, in: Respiration in Aquatic Ecosystems, edited by: del Giorgio, P. A. and Williams, P. J. le B., Oxford University Press, Oxford, 267–303, https://doi.org/10.1093/acprof:oso/9780198527084.003.0014, 2005.

Demers, S., Legendre, L., Maestrini, S. Y., Rochet, M., and Ingram, R. G.: Nitrogenous nutrition of sea-ice microalgae, Polar Biol., 9, 377–383, https://doi.org/10.1007/BF00442528, 1989.

Dezutter, T., Lalande, C., Darnis, G., and Fortier, L.: Seasonal and interannual variability of the Queen Maud Gulf ecosystem derived from sediment trap measurements, Limnol. Oceanogr., 66, S411–S426, https://doi.org/10.1002/lno.11628, 2020.

Duarte, P., Assmy, P., Campbell, K., and Sundfjord, A.: The importance of turbulent ocean–sea ice nutrient exchanges for simulation of ice algal biomass and production with CICE6.1 and Icepack 1.2, Geosci. Model Dev., 15, 841–857, https://doi.org/10.5194/gmd-15-841-2022, 2022.

Duarte, P., Meyer, A., and Moreau, S.: Nutrients in water masses in the Atlantic sector of the Arctic Ocean: temporal trends, mixing and links with primary production, J. Geophys. Res. Oceans, 126, e2021JC017413, https://doi.org/10.1029/2021JC017413, 2021.

Duarte, P., Sundfjord, A., Meyer, A., Hudson, S. R., Spreen, G., and Smedsrud, L.: Warm Atlantic water explains observed sea ice melt rates north of Svalbard, J. Geophys. Res. Oceans, 125, e2019JC015662, https://doi.org/10.1029/2019JC015662, 2020.

Durkin, C. A., Bender, S. J., Chan, K. Y. K., Gaessner, K., Grünbaum, D., and Armbrust, E. V.: Silicic acid supplied to coastal diatom communities influences cellular silicification and the potential export of carbon, Limnol. Oceanogr., 58, 1707–1726, https://doi.org/10.4319/lo.2013.58.5.1707, 2013.

Dybwad, C., Lalande, C., Bodur, Y. V., Henley, S. F., Cottier, F., Ershova, E. A., Hobbs, L., Last, K. S., Dąbrowska, A. M., and Reigstad, M.: The influence of sea ice cover and Atlantic water advection on annual particle export north of Svalbard, J. Geophys. Res. Oceans, 127, e2022JC018897, https://doi.org/10.1029/2022JC018897, 2022.

Ehrlich, J., Schaafsma, F. L., Bluhm, B. A., Peeken, I., Castellani, G., Brandt, A., and Flores, H.: Sympagic Fauna in and Under Arctic Pack Ice in the Annual Sea-Ice System of the New Arctic, Front. Mar. Sci., 7, 452, https://doi.org/10.3389/fmars.2020.00452, 2020.

https://doi.org/10.5194/egusphere-2026-4031
Preprint. Discussion started: 15 July 2026

Ehrlich, J., Bluhm, B. A., Peeken, I., Massicotte, P., Schaafsma, F. L., Castellani, G., Brandt, A., and Flores, H.: Sea-ice associated carbon flux in Arctic spring, Elem. Sci. Anthr., 9, 00169, https://doi.org/10.1525/elementa.2020.00169, 2021.

Fenchel, T. and Glud, R. N.: Benthic primary production and O_2–CO_2 dynamics in a shallow-water sediment: spatial and temporal heterogeneity, Ophelia, 53, 159–171, https://doi.org/10.1080/00785236.2000.10409446, 2000.

Fernández-Méndez, M., Wenzhöfer, F., Peeken, I., Sørensen, H. L., Glud, R. N., and Boetius, A.: Composition, buoyancy regulation and fate of ice algal aggregates in the central Arctic Ocean, PLoS ONE, 9, e107452, https://doi.org/10.1371/journal.pone.0107452, 2014.

Fernández-Méndez, M., Katlein, C., Rabe, B., Nicolaus, M., Peeken, I., Bakker, K., Flores, H., and Boetius, A.: Photosynthetic production in the central Arctic Ocean during the record sea-ice minimum in 2012, Biogeosciences, 12, 3525–3549, https://doi.org/10.5194/bg-12-3525-2015, 2015.

Fong, A. A., Hoppe, C. J. M., Aberle, N., Ashjian, C. J., Assmy, P., Bai, Y., Bakker, D. C. E., Balmonte, J. P., Barry, K. R., Bertilsson, S., et al.: Overview of the MOSAiC expedition: ecosystem, Elem. Sci. Anthr., 12, 00135, https://doi.org/10.1525/elementa.2023.00135, 2024.

Fripiat, F., Meiners, K. M., Vancoppenolle, M., Papadimitriou, S., Thomas, D. N., Ackley, S. F., Arrigo, K. R., Carnat, G., Cozzi, S., Delille, B., Dieckmann, G. S., Dunbar, R. B., Fransson, A., Kattner, G., Kennedy, H., Lannuzel, D., Munro, D. R., Nomura, D., Rintala, J. M., Schoemann, V., Stefels, J., Steiner, N., and Tison, J.-L.: Macro-nutrient concentrations in Antarctic pack ice: Overall patterns and overlooked processes, Elem. Sci. Anthr., 5, 13, https://doi.org/10.1525/elementa.217, 2017.

Fukami, H., Kojima, K., and Aburakawa, H.: The extinction and absorption of solar radiation within a snow cover, *Ann. Glaciol.*, 6, 118–122, https://doi.org/10.3189/1985AoG6-1-118-122, 1985.

Gasol, J. M. and Morán, X. A. G.: Flow cytometric determination of microbial abundances and its use to obtain indices of community structure and relative activity, in: Hydrocarbon and Lipid Microbiology Protocols: Single-Cell and Single-Molecule Methods, edited by: McGenity, T. J., Timmis, K. N., and Nogales, B., Springer, Berlin, Heidelberg, 159–187, https://doi.org/10.1007/8623_2015_139, 2016.

Geider, R. J. and La Roche, J.: Redfield revisited: Variability of C:N:P in marine microalgae and its biochemical basis, Eur. J. Phycol., 37, 1–17, https://doi.org/10.1017/S0967026201003456, 2002.

Goodman, L., Levine, E. R., and Lueck, R. G.: On measuring the terms of the turbulent kinetic energy budget from an AUV, *J. Atmos. Ocean. Technol.*, 23(7), 977–990, 2006, https://doi.org/10.1175/jtech1889.1.

Gordon, D. C., Jr.: Examination of methods of particulate organic carbon analysis, Deep-Sea Res., 16, 661–665, 1969.

Gradinger, R., and Bluhm, B. A.: First analysis of an Arctic sea ice meiofauna food web based on abundance, biomass and stable isotope ratios, *Mar. Ecol. Prog. Ser.*, 634, 29–43, https://doi.org/10.3354/meps13170, 2020.

Graham, R. M., Itkin, P., Meyer, A., Sundfjord, A., Spreen, G., Smedsrud, L. H., Liston, G. E., Cheng, B., Cohen, L., Divine, D., Fer, I., Fransson, A., Gerland, S., Haapala, J., Hudson, S. R., Johansson, A. M., King, J., Merkouriadi, I., Peterson, A. K., Provost, C., Randelhoff, A., Rinke, A., Rösel, A., Sennéchael, N., Walden, V. P., Duarte, P., Assmy, P., Steen, H., and Granskog, M. A.: Winter storms accelerate the

https://doi.org/10.5194/egusphere-2026-4031
Preprint. Discussion started: 15 July 2026

demise of sea ice in the Atlantic sector of the Arctic Ocean, Sci. Rep., 9, 9222, https://doi.org/10.1038/s41598-019-45574-5, 2019.

Gregg, M. C., D'Asaro, E. A., Riley, J. J., and Kunze, E.: Mixing efficiency in the ocean, *Annu. Rev. Mar. Sci.*, 10, 443–473, https://doi.org/10.1146/annurev-marine-121916-063643, 2018.

Grenfell, T. C., and Maykut, G. A.: The optical properties of ice and snow in the Arctic Basin, *J. Glaciol.*, 18(80), 445–463, https://doi.org/10.3189/S0022143000021122, 1977.

Hansen, H. P., and Koroleff, F.: Determination of nutrients, in: *Methods of Seawater Analysis*, John Wiley & Sons, Ltd., 159–228, https://doi.org/10.1002/9783527613984.ch10, 1999.

Hegseth, E. N. and von Quillfeldt, C. H.: The sub-ice algal communities of the Barents Sea pack ice: temporal and spatial distribution of biomass and species, J. Mar. Sci. Eng., 10, 164, https://doi.org/10.3390/jmse10020164, 2022.

Henley, S. F., Porter, M., Hobbs, L., Braun, J., Guillaume-Castel, R., Venables, E. J., Dumont, E., and Cottier, F.: Nitrate supply and uptake in the Atlantic Arctic sea ice zone: seasonal cycle, mechanisms and drivers, *Philos. Trans. R. Soc. A*, 378(2181), 20190361, 2020, https://doi.org/10.1098/rsta.2019.0361.

Heorton, H. D. B. S., Stroeve, J. C., and Veyssière, G.: Future under-sea-ice light availability and algal bloom timing from CMIP6 model simulations, Front. Mar. Sci., 12, 1642506, https://doi.org/10.3389/fmars.2025.1642506, 2025.

Hu, Y.-B., Wang, F., Boone, W., Barber, D., and Rysgaard, S.: Assessment and improvement of the sea ice processing for dissolved inorganic carbon analysis, *Limnol. Oceanogr. Methods*, 16(2), 83–91, https://doi.org/10.1002/lom3.10229, 2018.

Ingvaldsen, R. B., Assmann, K. M., Primicerio, R., Fossheim, M., Polyakov, I. V., and Dolgov, A. V.: Physical manifestations and ecological implications of Arctic Atlantification, Nat. Rev. Earth Environ., 2, 874–889, https://doi.org/10.1038/s43017-021-00228-x, 2021.

Itkin, P., Hendricks, S., Webster, M., von Albedyll, L., Arndt, S., Divine, D., Jaggi, M., Oggier, M., Raphael, I., Ricker, R., Rohde, J., Schneebeli, M., and Liston, G. E.: Sea ice and snow characteristics from year-long transects at the MOSAiC Central Observatory, Elem. Sci. Anthr., 11, 00048, https://doi.org/10.1525/elementa.2022.00048, 2023.

Itkin, P., Salganik, E., Divine, D. V., Jutila, A., Katlein, C., Neudert, M., Raphael, I. A., and Ricker, R.: Year-round assessment of sea ice pressure ridges by multi-frequency electromagnetic induction sounding, EGUsphere [preprint], https://doi.org/10.5194/egusphere-2025-6081, 2025.

Jakobsson, M., Mayer, L., Coakley, B., Dowdeswell, J. A., Forbes, S., Fridman, B., Hodnesdal, H., Noormets, R., Pedersen, R., Rebesco, M., Schenke, H. W., Zarayskaya, Y., Accettella, D., Armstrong, A., Anderson, R.M., Bienhoff, P., Camerlenghi, A., Church, I., Edwards, M., Gardner, J.V., Hall, J.K., Hell, B., Hestvik, O., Kristoffersen, Y., Marcussen, C., Mohammad, R., Mosher, D., Nghiem, S.V., Pedrosa, M.T., Travaglini, P.G., and Weatheral, P.: The International Bathymetric Chart of the Arctic Ocean (IBCAO) version 3.0, Geophys. Res. Lett., 39, L12609, https://doi.org/10.1029/2012GL052219, 2012.

Jassby, A. D. and Platt, T.: Mathematical formulation of the relationship between photosynthesis and light for phytoplankton, Limnol. Oceanogr., 21, 540–547, https://doi.org/10.4319/lo.1976.21.4.0540, 1976.

https://doi.org/10.5194/egusphere-2026-4031
Preprint. Discussion started: 15 July 2026

945 Katlein, C., Arndt, S., Belter, H. J., Castellani, G., and Nicolaus, M.: Seasonal evolution of light transmission distributions through Arctic sea ice, J. Geophys. Res. Oceans, 124, 5418–5435, https://doi.org/10.1029/2018JC014833, 2019.

Koch, C. W., Brown, T. A., Amiraux, R., Ruiz-Gonzalez, C., MacCorquodale, M., Yunda-Guarin, G. A., Kohlbach, D., Loseto, L. L., Rosenberg, B., Hussey, N. E., Ferguson, S. H., and Yurkowski, D. J.: Year-
950 round utilization of sea ice-associated carbon in Arctic ecosystems, Nat. Commun., 14, 1964, https://doi.org/10.1038/s41467-023-37612-8, 2023.

Koenig, Z., Provost, C., Sennéchael, N., Garric, G., and Gascard, J.-C.: The Yermak Pass Branch: a major pathway for the Atlantic Water north of Svalbard?, J. Geophys. Res. Oceans, 122, 9332–9349, https://doi.org/10.1002/2017JC013271, 2017.

955 Koenig, Z., Kolås, E. H., and Fer, I.: Structure and drivers of ocean mixing north of Svalbard in summer and fall 2018, Ocean Sci., 17, 365–381, https://doi.org/10.5194/os-17-365-2021, 2021.

Koenig, Z., Fer, I., Chierici, M., Fransson, A., Jones, E., and Kolås, E. H.: Diffusive and advective cross-frontal fluxes of inorganic nutrients and dissolved inorganic carbon in the Barents Sea in autumn, Prog. Oceanogr., 219, 103161, https://doi.org/10.1016/j.pocean.2023.103161, 2023.

960 Kolås, E. H., Koenig, Z., Fer, I., Nilsen, F., and Marnela, M.: Structure and transport of Atlantic Water north of Svalbard from observations in summer and fall 2018, J. Geophys. Res. Oceans, 125, e2020JC016174, https://doi.org/10.1029/2020JC016174, 2020.

Kowalczuk, P., Meler, J., Kauko, H. M., Pavlov, A. K., Zabłocka, M., Peeken, I., Dybwad, C., Castellani, G., and Granskog, M. A.: Bio-optical properties of Arctic drift ice and surface waters north of Svalbard from
965 winter to spring, J. Geophys. Res. Oceans, 122, 4634–4660, https://doi.org/10.1002/2016JC012589, 2017.

Krause, J. W., Duarte, C. M., Marquez, I. A., Assmy, P., Fernández-Méndez, M., Wiedmann, I., Wassmann, P., Kristiansen, S., and Agustí, S.: Biogenic silica production and diatom dynamics in the Svalbard region during spring, Biogeosciences, 15, 6503–6517, https://doi.org/10.5194/bg-15-6503-2018, 2018.

970 Krisch, S., Browning, T. J., Graeve, M., Ludwichowski, K.-U., Lodeiro, P., Hopwood, M. J., Roig, S., Yong, J.-C., Kanzow, T., and Achterberg, E. P.: The influence of Arctic Fe and Atlantic fixed N on summertime primary production in Fram Strait, North Greenland Sea, Sci. Rep., 10, 15230, https://doi.org/10.1038/s41598-020-72100-9, 2020.

Kvernvik, A. C., Hoppe, C. J. M., Greenacre, M., Verbiest, S., Wiktor, J. M., Gabrielsen, T. M., Reigstad, M.,
975 and Leu, E.: Arctic sea ice algae differ markedly from phytoplankton in their ecophysiological characteristics, Mar. Ecol. Prog. Ser., 666, 31–55, https://doi.org/10.3354/meps13675, 2021.

Kwok, R., Kacimi, S., Webster, M. A., Kurtz, N. T., and Petty, A. A.: Arctic snow depth and sea ice thickness from ICESat-2 and CryoSat-2 freeboards: A first examination, J. Geophys. Res. Oceans, 125, e2019JC016008, https://doi.org/10.1029/2019JC016008, 2020.

980 Lange, B. A., Katlein, C., Nicolaus, M., Peeken, I., and Flores, H.: Sea ice algae chlorophyll a concentrations derived from under-ice spectral radiation profiling platforms, J. Geophys. Res. Oceans, 121, 8511–8534, https://doi.org/10.1002/2016JC011991, 2016.

https://doi.org/10.5194/egusphere-2026-4031
Preprint. Discussion started: 15 July 2026

Lange, B. A., Katlein, C., Fernández-Méndez, I., Peeken, I., Schüller, D., and Flores, H.: *Sea ice algae chlorophyll a concentrations derived from under-ice spectral radiation profiling platforms*, J. Geophys. Res. Oceans, 121, 8249–8268, https://doi.org/10.1002/2016JC011991, 2016.

Lannuzel, D., Tedesco, L., van Leeuwe, M., Campbell, K., Flores, H., Delille, B., Miller, L., Stefels, J., Assmy, P., Bowman, J., et al.: The future of Arctic sea-ice biogeochemistry and ice-associated ecosystems, *Nat. Clim. Change*, 10(11), 983–992, 2020, https://doi.org/10.1038/s41558-020-00940-4.

Lavoie, D., Denman, K., and Michel, C.: Modeling ice algal growth and decline in a seasonally ice-covered region of the Arctic (Resolute Passage, Canadian Archipelago), J. Geophys. Res. Oceans, 110, C11009, https://doi.org/10.1029/2005JC002922, 2005.

Lei, R., Cheng, B., Hoppmann, M., Zhang, F., Zuo, G., Hutchings, J. K., Lin, L., Lan, M., Wang, H., Regnery, J., Krumpen, T., Haapala, J., Rabe, B., Perovich, D. K., and Nicolaus, M.: Seasonality and timing of sea ice mass balance and heat fluxes in the Arctic transpolar drift during 2019–2020, Elem. Sci. Anthr., 10, 000089, https://doi.org/10.1525/elementa.2021.000089, 2022.

Leu, E., Mundy, C. J., Assmy, P., Campbell, K., Gabrielsen, T. M., Gosselin, M., Juul-Pedersen, T., and Gradinger, R.: Arctic spring awakening – steering principles behind the phenology of vernal ice algal blooms, Prog. Oceanogr., 139, 151–170, https://doi.org/10.1016/j.pocean.2015.07.012, 2015.

Lewis, C., Schiffrine, N., Gosselin, M., Rochon, A., Amagoalik, J., Aariak, U. J., Galley, R., Lessard, S., and Niemi, A.: Multi-year assessment of coastal sea-ice algae and phytoplankton in an Arctic port ecosystem, Nunavut, Canada, *Arct. Sci.*, 12, 1–17, https://doi.org/10.1139/as-2025-0034, 2026.

Lueck, R. G.: The statistics of oceanic turbulence measurements. Part I: Shear variance and dissipation rates, J. Atmos. Oceanic Technol., 39, 1259–1271, https://doi.org/10.1175/JTECH-D-21-0051.1, 2022.

Lund-Hansen, L. C., Hawes, I., Hancke, K., Salmansen, N., Nielsen, J. R., Balslev, L., and Sorrell, B. K.: Effects of increased irradiance on biomass, photobiology, nutritional quality, and pigment composition of Arctic sea ice algae, Mar. Ecol. Prog. Ser., 648, 95–110, https://doi.org/10.3354/meps13411, 2020.

Macfarlane, A. R., Schneebeli, M., Dadic, R., Tavri, A., Immerz, A., Polashenski, C., Krampe, D., Clemens-Sewall, D., Wagner, D. N., Perovich, D. K., Hannula, H.-R., Raphael, I., Matero, I., Regnery, J., Smith, M. M., Nicolaus, M., Jaggi, M., Oggier, M., Webster, M. A., Lehning, M., Kolabutin, N., Itkin, P., Naderpour, R., Pirazzini, R., Hämmerle, S., Arndt, S., and Fons, S.: A database of snow on sea ice in the central Arctic collected during the MOSAiC expedition, Sci. Data, 10, 398, https://doi.org/10.1038/s41597-023-02273-1, 2023.

Mallett, R. D. C., Stroeve, J. C., Tsamados, M., Willatt, R., Newman, T., Nandan, V., Landy, J., Itkin, P., Oggier, M., Jaggi, M., and Perovich, D.: Sub-kilometre scale distribution of snow depth on Arctic sea ice from Soviet drifting stations, J. Glaciol., 68, 1014–1026, https://doi.org/10.1017/jog.2022.18, 2022.

Matthes, L. C., Mundy, C. J., Lambert-Girard, S., Babin, M., Vérin, G., and Ehn, J. K.: Spatial heterogeneity as a key variable influencing spring–summer progression in UVR and PAR transmission through Arctic sea ice, Front. Mar. Sci., 7, 183, https://doi.org/10.3389/fmars.2020.00183, 2020.

McKay, R. D., Koenig, Z., Duarte, P., Gradinger, R., Else, B., Osanen, J. E., and Campbell, K.: Influence of oceanic mixing on sea ice net community production in the Canadian Arctic, *Elem. Sci. Anthr.*, [accepted], 2026.

https://doi.org/10.5194/egusphere-2026-4031
Preprint. Discussion started: 15 July 2026

McNair, H. M., Brzezinski, M. A., and Krause, J. W.: Diatom populations in an upwelling environment decrease silica content to avoid growth limitation, Environ. Microbiol., 20, 4184–4193, https://doi.org/10.1111/1462-2920.14431, 2018.

McNutt, S. L. and Overland, J. E.: Spatial hierarchy in Arctic sea ice dynamics, Tellus A, 55, 181–191, https://doi.org/10.1034/j.1600-0870.2003.00012.x, 2003.

Medlin, L. K. and Priddle, J.: Polar Marine Diatoms, Cambridge University Press, Cambridge, 1990.

Merkouriadi, I., Cheng, B., Graham, R. M., Rösel, A., and Granskog, M. A.: Critical role of snow on sea ice growth in the Atlantic sector of the Arctic Ocean, Geophys. Res. Lett., 44, 10479–10485, https://doi.org/10.1002/2017GL075494, 2017.

Merkouriadi, I., Cheng, B., Hudson, S. R., and Granskog, M. A.: Effect of frequent winter warming events (storms) and snow on sea-ice growth – a case from the Atlantic sector of the Arctic Ocean during the N-ICE2015 campaign, Ann. Glaciol., 61, 164–170, https://doi.org/10.1017/aog.2020.25, 2020.

Meyer, A., Sundfjord, A., Fer, I., Provost, C., Villacieros Robineau, N., Koenig, Z., Onarheim, I. H., Smedsrud, L. H., Duarte, P., Dodd, P. A., Graham, R. M., Schmidtko, S., and Kauko, H. M.: Winter to summer oceanographic observations in the Arctic Ocean north of Svalbard, J. Geophys. Res. Oceans, 122, 6218–6237, https://doi.org/10.1002/2016JC012391, 2017.

Meyer, A., Fer, I., Sundfjord, A., and Peterson, A. K.: Mixing rates and vertical heat fluxes north of Svalbard from Arctic winter to spring, J. Geophys. Res. Oceans, 122, 4569–4586, https://doi.org/10.1002/2016JC012441, 2017.

Mundy, C. J., Barber, D. G., and Michel, C.: Variability of snow and ice thermal, physical and optical properties pertinent to sea ice algae biomass during spring, J. Mar. Syst., 58, 107–120, https://doi.org/10.1016/j.jmarsys.2005.07.003, 2005.

Mundy, C. J., Leu, E., Campbell, K., Galindo, V., Levasseur, M., Poulin, M., Tremblay, J.-É., and Gosselin, M.: Intracellular nutrient storage during ice algal spring blooms in the Canadian high Arctic, iScience, 28, 113148, https://doi.org/10.1016/j.isci.2025.113148, 2025.

Nicolaus, M., Katlein, C., Maslanik, J., and Hendricks, S.: Changes in Arctic sea ice result in increasing light transmittance and absorption, Geophys. Res. Lett., 39, L24501, https://doi.org/10.1029/2012GL053738, 2012.

Nicolaus, M., Petrich, C., Hudson, S. R., and Granskog, M. A.: Variability of light transmission through Arctic land-fast sea ice during spring, The Cryosphere, 7, 977–986, https://doi.org/10.5194/tc-7-977-2013, 2013.

Norwegian Meteorological Institute: Arctic Shipborne Sea Ice Standardization Tool (ASSIST), available at: https://cryo.met.no/en/icewatch (last access: 28 May 2023).

Olsen, L. M., Laney, S. R., Duarte, P., Kauko, H. M., Fernández-Méndez, M., Mundy, C. J., Rösel, A., Meyer, A., Itkin, P., Cohen, L., Peeken, I., Tatarek, A., Różańska-Pluta, M., Wiktor, J., Taskjelle, T., Pavlov, A. K., Hudson, S. R., Granskog, M. A., Hop, H., and Assmy, P.: The seeding of ice algal blooms in Arctic pack ice: the multiyear ice seed repository hypothesis, J. Geophys. Res. Biogeosci., 122, 1529–1548, https://doi.org/10.1002/2016JG003668, 2017.

Osborn, J. W.: Estimates of the local rate of vertical diffusion from dissipation measurements, J. Phys. Oceanogr., 10, 83–89, https://doi.org/10.1175/1520-0485(1980)010<0083:EOTLRO>2.0.CO;2, 1980.

https://doi.org/10.5194/egusphere-2026-4031
Preprint. Discussion started: 15 July 2026

Oziel, L., Baudena, A., Ardyna, M., Massicotte, P., Randelhoff, A., Sallée, J.-B., Ingvaldsen, R. B., Devred, E., and Babin, M.: Faster Atlantic currents drive poleward expansion of temperate phytoplankton in the Arctic Ocean, Nat. Commun., 11, 1705, https://doi.org/10.1038/s41467-020-15485-5, 2020.

Parsons, T. R., Maita, Y., and Lalli, C. M.: Plankton preservatives, in: *A Manual of Chemical and Biological Methods for Seawater Analysis*, edited by: Parsons, T. R., Maita, Y., and Lalli, C. M., Pergamon, Amsterdam, 163–164, https://doi.org/10.1016/B978-0-08-030287-4.50048-7, 1984.

Perovich, D. K.: *The Optical Properties of Sea Ice*, U.S. Army Cold Regions Research & Engineering Laboratory Monograph 96-1, Hanover, NH, USA, 1996.

Perovich, D. K.: Light reflection and transmission by a temperate snow cover, *J. Glaciol.*, 53(181), 201–210, https://doi.org/10.3189/172756507782202919, 2007.

Peterson, A. K., Fer, I., McPhee, M. G. and Randelhoff, A.: Turbulent heat and momentum fluxes in the upper ocean under Arctic sea ice, *J. Geophys. Res. Oceans*, 122(2), 1439–1456, https://doi.org/10.1002/2016JC012283, 2017.

Platt, T., Gallegos, C. L., and Harrison, W. G.: Photoinhibition of photosynthesis in natural assemblages of marine phytoplankton, *J. Mar. Res.*, 38, 687–701, 1980.

Polyakov, I. V., Pnyushkov, A. V., Alkire, M. B., Ashik, I. M., Baumann, T. M., Carmack, E. C., Goszczko, I., Guthrie, J., Ivanov, V. V., Kanzow, T., et al.: Greater role for Atlantic inflows on sea-ice loss in the Eurasian Basin of the Arctic Ocean, *Science*, 356(6335), 285–291, https://doi.org/10.1126/science.aai8204, 2017.

Poulin, M., and Cardinal, A.: Sea ice diatoms from Manitounuk Sound, southeastern Hudson Bay (Quebec, Canada). III. Cymbellaceae, Entomoneidaceae, Gomphonemataceae, and Nitzschiaceae, *Can. J. Bot.*, 61(1), 107–118, https://doi.org/10.1139/b83-010, 1983.

Raymond, P. A., and Bauer, J. E.: Riverine export of aged terrestrial organic matter to the North Atlantic Ocean, *Nature*, *409*(6819), 497–500, https://doi.org/10.1038/35054034, 2001.

Redfield, A. C., Ketchum, B. H., and Richards, F. A.: The influence of organisms on the composition of seawater, in: *The Sea*, edited by: Hill, M. N., John Wiley, New York, 26–77, 1963.

Renner, A. H. H., Bailey, A., Reigstad, M., Sundfjord, A., Chierici, M., and Jones, E. M.: Hydrography, inorganic nutrients and chlorophyll *a* linked to sea ice cover in the Atlantic Water inflow region north of Svalbard, *Prog. Oceanogr.*, **219**, 103162, https://doi.org/10.1016/j.pocean.2023.103162, 2023.

Rochet, M., Legendre, L., and Demers, S.: Photosynthetic and pigment responses of sea-ice microalgae to changes in light intensity and quality, *J. Exp. Mar. Biol. Ecol.*, **101**, 211–226, https://doi.org/10.1016/0022-0981(86)90264-9, 1986.

Rysgaard, S., Kuhl, M., Glud, R. N., and Hansen, J. W.: Biomass, production and horizontal patchiness of sea ice algae in a high-Arctic fjord (Young Sound, NE Greenland), *Mar. Ecol. Prog. Ser.*, **223**, 15–26, https://doi.org/10.3354/meps223015, 2001.

Salganik, E., Lange, B. A., Itkin, P., Divine, D., Katlein, C., Nicolaus, M., Hoppmann, M., Neckel, N., Ricker, R., Høyland, K. V., et al.: Different mechanisms of Arctic first-year sea-ice ridge consolidation observed during the MOSAiC expedition, *Elem. Sci. Anthr.*, **11**(1), 00008, https://doi.org/10.1525/elementa.2023.00008, 2023.

https://doi.org/10.5194/egusphere-2026-4031
Preprint. Discussion started: 15 July 2026

Schulz, K., Koenig, Z., Muilwijk, M., Bauch, D., Hoppe, C. J. M., Droste, E. S., Hoppmann, M., Chamberlain, E. J., Laukert, G., Stanton, T., Quintanilla-Zurita, A., Fer, I., Heuzé, C., Karam, S., Mieruch-Schnülle, S., Baumann, T. M., Vredenborg, M., Tippenhauer, S., and Granskog, M. A.: The Eurasian Arctic Ocean along the MOSAiC drift in 2019–2020: an interdisciplinary perspective on physical properties and processes, *Elem. Sci. Anthr.*, **12**(1), 00114, https://doi.org/10.1525/elementa.2023.00114, 2024.

Shiozaki, T., Ijichi, M., Fujiwara, A., Makabe, A., Nishino, S., Yoshikawa, C., and Harada, N.: Factors regulating nitrification in the Arctic Ocean: potential impact of sea ice reduction and ocean acidification, *Glob. Biogeochem. Cycles*, **33**, 1085–1099, https://doi.org/10.1029/2018GB006068, 2019.

Smith, M. M., Fuchs, N., Salganik, E., Perovich, D. K., Raphael, I., Granskog, M. A., Schulz, K., Shupe, M. D., and Webster, M.: Formation and fate of freshwater on an ice floe in the Central Arctic, *The Cryosphere*, **19**(2), 619–644, https://doi.org/10.5194/tc-19-619-2025, 2025.

Strickland, J. D. H., and Parsons, T. R.: *A Practical Handbook of Seawater Analysis*, Fisheries Research Board of Canada, Ottawa, 1972.

Sundfjord, A., Assmann, K. M., Lundesgaard, Ø., Renner, A. H. H., Lind, S., and Ingvaldsen, R. B.: Suggested water mass definitions for the central and northern Barents Sea, and the adjacent Nansen Basin: workshop report, *Nansen Legacy Report Series*, 8, https://doi.org/10.7557/nlrs.5707, 2020.

Thielecke, A. U., Hoppe, C. J. M., Krause, J. W., Eggers, S. L., John, U., Clarke, D., Whitehouse, M., Jeon, H., Caputo, N., Cucchi, F., Curtin, A., and Fernández-Méndez, M.: From *Phaeocystis* to *Chaetoceros*: silicic acid as the primary driver of diatom bloom magnitude in an Arctic mesocosm experiment, *EGUsphere* [preprint], 1–51, https://doi.org/10.5194/egusphere-2026-3186, 2026.

Timmermans, M.-L., and Marshall, J.: Understanding Arctic Ocean circulation: a review of ocean dynamics in a changing climate, *J. Geophys. Res. Oceans*, **125**(4), e2018JC014378, https://doi.org/10.1029/2018JC014378, 2020.

Tomas, C. R.: *Identifying Marine Phytoplankton*, Academic Press, San Diego, 1997.

Veyssière, G., Castellani, G., Wilkinson, J., Karcher, M., Hayward, A., Stroeve, J. C., Nicolaus, M., Kim, J.-H., Yang, E.-J., Valcic, L., et al.: Under-ice light field in the western Arctic Ocean during late summer, *Front. Earth Sci.*, **9**, 643737, https://doi.org/10.3389/feart.2021.643737, 2022.

von Albedyll, L., Hendricks, S., Hutter, N., Murashkin, D., Kaleschke, L., Willmes, S., Thielke, L., Tian-Kunze, X., Spreen, G., and Haas, C.: Lead fractions from SAR-derived sea ice divergence during MOSAiC, *The Cryosphere*, **18**(3), 1259–1285, https://doi.org/10.5194/tc-18-1259-2024, 2024.

Vonnahme, T. R., Leroy, M., Thoms, S., van Oevelen, D., Harvey, H. R., Kristiansen, S., Gradinger, R., Dietrich, U., and Völker, C.: Modeling silicate–nitrate–ammonium co-limitation of algal growth and the importance of bacterial remineralization based on an experimental Arctic coastal spring bloom culture study, *Biogeosciences*, **18**(5), 1719–1747, https://doi.org/10.5194/bg-18-1719-2021, 2021.

Webster, M. A., Liu, Z., Light, B., and Perovich, D. K.: A brighter Arctic Ocean: trends in solar partitioning in the Arctic sea ice–ocean system from 1984 to 2024, *Geophys. Res. Lett.*, **53**, e2025GL120478, https://doi.org/10.1029/2025GL120478, 2026.

Wolf, K. K. E., Rokitta, S. D., Hoppe, C. J. M., and Rost, B.: Pelagic and ice-associated microalgae under elevated light and pCO_2: contrasting physiological strategies in two Arctic diatoms, *Limnol. Oceanogr.*, **67**(9), 1895–1910, https://doi.org/10.1002/lno.12174, 2022.